Title:

VMHdm/c^{SF-1} Neuronal Circuits Regulate Skeletal Muscle PGC1-α via the Sympathoadrenal Drive

Author:

Takuya Yoshida[1,2*], Mina Fujitani[3, 4], Scotlynn Farmer[1], Ami Harada[1,5], Zhen Shi[1,6], Jenny J. Lee[3], Arely Tinajero[3], Ashish K. Singha[1], Teppei Fujikawa[1,3#]

Affiliation:

1. Department of Cellular and Integrative Physiology, Long School of Medicine, University of Texas Health San Antonio, San Antonio, US
2. Department of Clinical Nutrition School of Food and Nutritional Sciences, University of Shizuoka, Shizuoka, Japan
3. Center for Hypothalamic Research, Department of Internal Medicine, UT Southwestern Medical Center, Dallas, US
4. Laboratory of Nutrition Science, Department of Bioscience, Graduate School of Agriculture, Ehime University, Matsuyama, Japan
5. Nara Medical University, Nara, Japan
6. Department of Plastic Surgery, Hospital Zhejiang University School of Medicine, Zhejiang, China

*Current Address: Laboratory of Clinical Nutrition, Division of Food and Health Environmental Sciences, Prefectural University of Kumamoto, Kumamoto, Japan

Corresponding Author: Teppei Fujikawa email: teppei.fujikawa@utsouthwestern.edu

Abstract

Objective: To adapt to metabolically challenging environments, the central nervous system (CNS) orchestrates metabolism of peripheral organs including skeletal muscle. The organ-communication between the CNS and skeletal muscle has been investigated, yet our understanding of the neuronal pathway from the CNS to skeletal muscle is still limited. Neurons in the dorsomedial and central parts of the ventromedial hypothalamic nucleus (VMHdm/c) expressing steroidogenic factor-1 (VMHdm/c^{SF-1} neurons) are key for metabolic adaptations to exercise, including increased basal metabolic rate and skeletal muscle mass in mice. However, the mechanisms by which VMHdm/c^{SF-1} neurons regulate skeletal muscle function remain unclear. Here, we show that VMHdm/c^{SF-1} neurons increase the sympathoadrenal activity and regulate skeletal muscle peroxisome proliferator-activated receptor gamma coactivator 1 alpha (PGC-1α) in mice via multiple downstream nodes.

Methods: Optogenetics was used to specifically manipulate VMHdm/c^{SF-1} neurons combined with genetically-engineered mice and surgical manipulation of the sympathoadrenal activity.

Results: Optogenetic activation of VMHdm/c^{SF-1} neurons dramatically elevates mRNA levels of skeletal muscle *Pgc-1α*, which regulates a spectrum of skeletal muscle function including protein synthesis and metabolism. Mechanistically, the sympathoadrenal drive coupled with β2 adrenergic receptor (β2AdR) is essential for VMHdm/c^{SF-1} neurons-mediated increases in skeletal muscle PGC1-α. Specifically, both adrenalectomy and β2AdR knockout block augmented skeletal muscle PGC1-α by VMHdm/c^{SF-1} neuronal activation. Optogenetic functional mapping reveals that

48 downstream nodes of VMHdm/c^{SF-1} neurons are functionally redundant to increase circulating
49 epinephrine and skeletal muscle PGC1-α.
50
51 **Conclusions**: Collectively, we propose that VMHdm/c^{SF-1} neurons-skeletal muscle pathway,
52 VMHdm/c^{SF-1} neurons→multiple downstream nodes→the adrenal gland→skeletal muscle β2AdR,
53 underlies augmented skeletal muscle function for metabolic adaptations.

1. Introduction

The central nervous system (CNS) orchestrates the whole-body metabolism[1; 2]. Within the CNS, the hypothalamus plays a dominant role in the regulation of metabolic homeostasis in response to dynamic challenges such as hypoglycemia[3], cold-exposure[4], and exercise[5]. Our previous work articulates that neurons in the dorsomedial and central parts of ventromedial hypothalamic nucleus (VMHdm/c neurons) substantially contribute to metabolic adaptations to exercise training including augmented skeletal muscle mass and basal metabolic rate in mice[6]. Knockdown of steroidogenic factor-1 (SF-1)[7; 8] in VMHdm/c neurons hampers exercise-induced mRNA expression of *peroxisome proliferator-activated receptor gamma coactivator 1 alpha* (*Pgc-1α*) in skeletal muscle[6]. PGC-1α is a key transcriptional regulator that controls a broad range of genes related to glucose and fat metabolism, mitochondrial function, angiogenesis, and protein synthesis[9; 10]. Loss- or gain-of-function of PGC-1α in skeletal muscle dramatically changes skeletal muscle physiology as well as whole-body metabolism[11; 12]. These data suggest that VMHdm/c neurons expressing SF-1 (VMHdm/c^{SF-1} neurons) mediate metabolic responses of skeletal muscle to exercise, thereby contributing to metabolic benefits of exercise. However, the mechanisms by which VMHdm/c^{SF-1} neurons mediate exercise-induced augmented skeletal muscle PGC-1α expression remains unclear. In particular, the pathway from VMHdm/c^{SF-1} neurons to skeletal muscle has yet to be unraveled.

PGC-1α expression in skeletal muscle is augmented by a variety of physiological stimuli[9; 13]. For example, *ex vivo* muscle contraction is sufficient to increase mRNA levels of *Pgc-1α* by activation of calcium signaling pathways[14; 15]. Notably, the adrenergic activation such as epinephrine, norepinephrine, and β-2 adrenergic receptors (β2AdR) agonist can dramatically increase mRNA levels of *Pgc-1α* in skeletal muscle[16; 17]. In contrast, blocking the adrenergic

signaling by a systemic injection of β2AdR antagonist significantly hampers exercise-induced *Pgc-1α* mRNA in skeletal muscle[18]. Numerous studies have indicated that VMH neurons affect the sympathetic nervous system (SNS) activity[19; 20]. Knockdown of SF-1 in VMHdm/c neurons suppresses exercise-induced epinephrine release[6]. These data indicate that VMHdm/c^{SF-1} neurons regulate skeletal muscle PGC-1α via the SNS. However, the functional neurocircuits underlying VMHdm/c^{SF-1} neuronal regulation of the SNS are still unclear. A genetic labeling study using *Sf-1*-Cre mice, which express Cre-recombinase in VMHdm/c in adults, portraits that VMHdm/c neurons highly innervate to several areas that regulate the SNS activity, including the anterior bed nucleus of the stria terminalis (aBNST), preoptic area (POA), anterior hypothalamus area (AH), paraventricular hypothalamic nucleus (PVH), and periaqueductal gray (PAG)[21]. Although studies using optogenetics have identified that distinct downstream sites of VMHdm/c^{SF-1} neurons regulate blood glucose[22], defensive behaviors[23], and food intake[24], the vital downstream node of VMHdm/c^{SF-1} neurons regulating the SNS is unknown.

In this study, we used optogenetics and genetically-engineered mice to determine the key downstream nodes of VMHdm/c^{SF-1} neurons that regulate skeletal muscle PGC-1α via the SNS. We found that epinephrine release by the sympathoadrenal activity coupled with β2AdR is essential for VMHdm/c^{SF-1} neuronal-induced skeletal muscle PGC-1α. Furthermore, our results demonstrated that VMHdm/c^{SF-1} neurons regulate the SNS through functionally redundant circuits with the PVH and PAG acting as the main downstream nodes.

2. Material and Methods

2.1 Genetically-Engineered Mice

Sf-1-Cre mice were obtained from the Jackson Laboratory (US; Strain# 012462, RRID:IMSR_JAX:012462). *Abrb2* KO mice (RRID:IMSR_JAX:031496) were derived from β-null mice[25], which was kindly provided by Dr. Bradford Lowell (Harvard Medical School). The sequences of genotyping primers are followings; for *Sf-1*-Cre, aggaagcagccctggaac, aggcaaattttggtgtacgg, agaaactgctccgctttcc with expected bands sizes of 627 bp for internal control and 236 bp for *Sf-1*-Cre; for *Abrb2* knockout (KO), cacgagactagtgagacgtg, accaagaataaggcccgagt, ccgggaatagacaaagacca with expected bands sizes of 225 bp for the wild-type allele and 410 bp for the knockout allele. *Sf-1*-Cre and *Abrb2* KO mice were bred to generate *Sf-1*-Cre::*Abrb2*$^{KO/KO}$ and *Sf-1*-Cre::*Abrb2*$^{WT/WT}$ mice. *Sf-1*-Cre mice were on a C57BL/J6 background and other mice are on a mixed background (C57BL/J6 and FVB.129). We used 3-6 month-old male mice whose body weights were above approximately 25-30 grams. Mice were housed at room temperature (22–24℃) with a 12 hr light/dark cycle (lights on at 6am, and 7am during daylight saving time) and fed a normal chow diet (2016 Teklad global 16% protein rodent diets, Envigo, US). Mice were maintained in groups and singly housed after adeno-associated virus (AAV) injections and optic fiber probes insertions. Animal care was according to established NIH guidelines, and all procedures were approved by the Institutional Animal Care and Use Committee of the University of Texas Southwestern Medical Center and University of Texas Health San Antonio.

2.2 AAV injections and optic fiber probe insertions

118 Recombinant AAVs were purchased from the Vector Core at the University of North Carolina at
119 Chapel Hill, US or Addgene Inc (US). rAAV5-EF1α-DIO-mCherry (3.3 x 10^{12} VM/mL), rAAV5-
120 EF1α-DIO- channelrhodopsin2(ChR2)(H134R)-mCherry (3.4 x 10^{12} VM/mL), and rAAV5-EF1α-
121 DIO-ChR2(H134R)-EYFP (3.2 x 10^{12} VM/mL) were unilaterally administered into the right side
122 of the VMH of mice using a UMP3 UltraMicroPump (WPI, US) with 10 µL NanoFil microsyringe
123 (WPI) and 35G NanoFil beveled needle (WPI; Catalog# NF35BV-2). The volume of AAVs was
124 500-1000 nL at the rate 50-100 nL per minute, and the needle was left for another 5 minutes after
125 the injection was finished. The face of beveled needle was placed towards the center of the brain.
126 The coordinates of VMH-microinjection were AP; −1.4 L +0.5, and D −5.5 (from Bregma). The
127 optic fiber probe was inserted as following coordinates; the VMH (AP; −1.4, L +0.5, and D −5.0),
128 aBNST (AP; 0.3, L +0.5, and D −3.75), POA (AP; 0.4, L +0.25, and D −4.5), AH (AP; −0.9, L
129 +0.5, and D −4.75), PVH/AH (AP; −0.8, L +0.25, and D −4.5), and PAG (AP; −4.3, L +0.2, and
130 D −2.0). The configuration of the probe for the VMH stimulation was 400 µm Core, 0.5NA, Ø2.5
131 mm ceramic ferrule, and 6mm length (RWD Life science Inc, US and Doric Lenses, Canada) for
132 the LED input. The configuration of probe for other sites and the VMH (S Figure 4) was 200 µm
133 Core diameter, 0.39NA, Ø2.5 mm Ceramic Ferrule diameter, and with varied length varied (3-6
134 mm depending on the place) (RWD Life science Inc, US and Doric Lenses, Canada). The fiber
135 probe was secured by adhesion bond (Loctite 454, Loctite Inc, US). Mice were allowed to recover
136 for at least three weeks after the AAV injections to fully express recombinant proteins.
137

138 **2.3. Optogenetics**

139 The light emitting diode (LED) driver (Thorlabs, US; DC4104) with fiber-coupled LED (Thorlabs;
140 Catalog# M470F3) was used for the VMH stimulation, and the laser unit (Opto engine LLC, US;

141 Catalog# MDL-III-470) was used for the terminal of VMHdm/c^{SF-1} neuronal stimulations. The
142 power of tips was set to ~1 mW/mm^2 for the VMH stimulation and ~10 mW/mm^2 for the terminal
143 stimulations. The customed transistor-transistor logic generator was built based on the design by
144 the University of Colorado Optogenetics and Neural Engineering Core. Rotary joint patch cable
145 (Thorlabs; Catalog# RJPSF4 for LED and RJPFF4 for the laser) was used to connect either fiber-
146 coupled LED or the laser unit. The quick-release interconnect (Thorlabs; Catalog# ADAF2) was
147 used to connect the rotary joint patch cable to the fiber probe attached to mouse head. The
148 stimulation was set to; 5 ms duration, 20 Hz, 2 seconds activation and 2 seconds rest cycle, 30
149 minutes (Figure 1B) otherwise specified.
150

151 **2.4 Chemogenetics**

152 Gi-Designer Receptors Exclusively Activated by Designer Drugs (DREADDs)-AAV (Gi-
153 DREADD), rAAV8-hSyn-DIO-hM4D(Gi)-mCherry (Addgene Inc, Catalog# 44362-AAV8, 3.2 x
154 10^{12} VM/mL), was used for inhibition of VMHdm/c^{SF-1} neuronal activity induced by optogenetics.
155 rAAV8-hSyn-DIO-hM4D(Gi)-mCherry and rAAV5-EF1α-DIO-ChR2(H134R)-EYFP (250 nL
156 each, total 500 nL) were injected into the right side of the VMH of *Sf-1*-Cre mice as described
157 above. Control for rAAV5-EF1α-DIO-ChR2(H134R)-EYFP was rAAV5-EF1α-DIO-EYFP. The
158 optic cannula was inserted the VMH, PVH/AH or PAG as described above. Clozapine-N-Oxide
159 (CNO, catlog# HB6149, Hello Bio Inc, NJ, USA) was injected intraperitoneally (i.p.) 10 minutes
160 before optogenetic stimulation begun (2.5 mg/kg per BW). Sterile saline was used as vehicle and
161 control.
162

163 **2.5 Adrenalectomy (ADX)**

164 Skin and muscle incisions (approximately 1 cm) were made close to the abdominal area where
165 kidney was located. Both the adrenal glands were removed by tying with sterile suture. The sham
166 operation was performed as same as ADX surgery except for removing the adrenal glands. The
167 corticosterone water (75 µg/mL, vehicle was sterile 1% ethanol/0.9% NaCl water) was provided
168 with ADX mice, and vehicle was provided with sham mice.
169

170 **2.6 Immunohistochemistry and Fos counting**

171 Mouse brains were prepared as previously described[26; 27]. Anti-cFos (Sigma, US; Catalog#
172 F7799, batch #0000102540, RRID:AB_259739) and secondary fluorescent antibodies
173 (Thermofisher Inc, US; Catalog# A-21202, Lot#WF320931, and RRID:AB_141607; A-21203,
174 Lot#WD319534, and RRID:AB_141633; A10523, Lot# , and RRID:AB_1500679) were used.
175 Dilution rates for antibodies were 1:1000 for first antibody and 1:200 for second antibodies.
176 Images were captured by fluorescence microscopies (Keyence US, US; Model: BZ-X710, Leica
177 Inc, US; Model DM6 B). Exposure of captured images was adjusted, and each area (aBNST, POA,
178 AH, PVH, VMH, and PAG) was clipped by Photoshop based on the mouse brain atlas[28] .
179 Clipped images were exported to Fiji, and the number of cells expressing Fos was counted by
180 particle measurement function (Figure 5B).
181

182 **2.7 Assessment of glucose, catecholamines, and hormone levels in the blood**

183 Blood glucose was measured by a glucose meter as previously described[6; 27; 29]. Plasma
184 catecholamines and hormones levels were measured as previously described[6; 27]. Briefly, the
185 plasma catecholamines were analyzed by the Vanderbilt Hormone Assay & Analytical Services
186 Core. Plasma Glucagon (Mercodia Inc, US; Catalog#10-1281-01), insulin (Crystal Chem Inc, US;

187 Catalog# 90080), and corticosterone (Cayman Chemical, US; Catalog #501320) levels were
188 determined by commercially available ELISA kits.
189
190 **2.8 Assessment of mRNA**
191 mRNA levels in the tibialis anterior (TA) muscle were determined as previously described[30].
192 The sequences of the deoxy-oligonucleotides primers are: *Ppargc1a* total (5'
193 tgatgtgaatgacttggatacagaca, and 5' gctcattgttgtactggttggatatg), *Ppargc1a-1* (5'
194 ggacatgtgcagccaagactct, and 5' cacttcaatccacccagaaagct), *Ppargc1a-2* (5' ccaccagaatgagtgacatgga,
195 and 5' gttcagcaagatctgggcaaa), *Ppargc1a-3* (5' aagtgagtaaccggaggcattc, and 5'
196 ttcaggaagatctgggcaaaga), *Ppargc1a-4* (5' tcacaccaaacccacagaaa, and 5' ctggaagatatggcacat), and
197 *18S* (5' catgcagaacccacgacagta and 5' cctcacgcagcttgttgtcta).
198
199 **2.9 Data analysis and statistical design**
200 The data are represented as means ± S.E.M. GraphPad PRISM version 9 (GraphPad, US) was
201 used for the statistical analyses and $P<0.05$ was considered as a statistically significant
202 difference. A detailed analysis was described in Supplemental Table 1. The sample size was
203 decided based on previous publications[6; 26; 27; 29-34], and no power analysis was used.
204 Experiments were biologically replicated in Figure 1, 2, 3, and Figure 4B. Experiments for qPCR
205 were technically replicated. We did not carry out replicate experiments for data shown in Figure
206 4C-H and 5. Figures were generated by PRISM version 9, Illustrator 2021-23, and Photoshop
207 2021-23 (Adobe Inc, US).

208 **3. Results**

209

210 **3.1 Optogenetic VMHdm/c^{SF-1} neuronal activation induces skeletal muscle *Pgc-1α* mRNA**
211 **expression**

212 To determine the neuronal mechanism by which VMHdm/c^{SF-1} neurons regulate skeletal
213 muscle function via the SNS, we generated mice expressing ChR2(H134R)[35] specifically in
214 VMHdm/c^{SF-1} neurons by microinjection of AAV bearing Cre-dependent ChR2 fused with
215 fluorescent reporters (AAV-DIO-ChR2) into *Sf-1* Cre mice[36] (VMHdm/c^{SF-1}::ChR2, Figure 1A).
216 We used AAV containing Cre-dependent mCherry for control (VMHdm/c^{SF-1}::mCherry). We used
217 the following stimulation configurations; 5 ms duration, 20 Hz, 2 seconds activation/2 seconds
218 resting cycle for 30 minutes (Figure 1B). We confirmed that our optogenetic configuration
219 significantly induced Fos protein expression, a neuronal activation marker, in the stimulated side
220 of the VMHdm/c, but not in the non-stimulated side (Figure 1C). Similar to previous studies[22;
221 37; 38], VMHdm/c^{SF-1} neuronal activation increased blood glucose (Figure 1D). In addition, we
222 observed that VMHdm/c^{SF-1} neuronal activation induced increases in plasma glucagon without
223 changing plasma insulin levels (Figure 1E and F). Next, we determined whether VMHdm/c^{SF-1}
224 neuronal activation can induce transcriptional changes in skeletal muscle. PGC-1α is a key
225 transcriptional regulator for a spectrum of genes governing glucose and fat metabolism, oxidative
226 capacity, protein synthesis and degradation, and vascularization[9; 10; 13]. Importantly, *Pgc-1α*
227 mRNA induction can be used as a readout of exercise-related skeletal muscle transcriptional
228 changes because a single exercise training dramatically increases mRNA levels of *Pgc-1α[6; 13]*.
229 PGC-1α has several isoforms such as PGC1a-1, -2, -3 and -4[39]. We found that 30 minutes of
230 VMHdm/c^{SF-1} neuronal activation is sufficient to induce *Pgc-1α-2, -3,* and *-4* mRNA levels in TA

skeletal muscle (Figure 1G). We then measured plasma catecholamines levels after VMHdm/c^{SF-1} neuronal activation. Interestingly, plasma epinephrine levels were significantly increased by VMHdm/c^{SF-1} neuronal activation, but norepinephrine levels in VMHdm/c^{SF-1} neuronal activated mice were not significantly different from control group (Figure 1 H and I). The increased epinephrine likely caused suppression of insulin secretion while mice showed hyperglycemia. Previous studies have shown that optogenetic VMHdm/c^{SF-1} neuronal activation elicits behavioral changes such as freeze and burst activity (combination of freeze, jump, and run)[23; 40]. In line with that, we found that VMHdm/c^{SF-1} neuronal activation induced freeze or burst activity (17 cases of freeze (55%), 14 cases of burst activity (45%); total 31 trials). However, we did not observe any differences of skeletal muscle *Pgc-1α* mRNA levels between mice showed freeze and burst activity (SFigure 1), suggesting that the burst activity is unlikely to contribute to VMHdm/c^{SF-1} neurons-induced *Pgc-1α* expression. Collectively, these data indicate that VMHdm/c^{SF-1} neurons regulate skeletal muscle function via sympathoadrenal activity, as the adrenal gland is the only organ able to secret epinephrine into circulation.

3.2 The adrenal gland is essential for VMHdm/c^{SF-1} neuronal regulation of skeletal muscle

Next, to determine whether epinephrine release from the adrenal gland is required for VMHdm/c^{SF-1} neurons-induced skeletal muscle *Pgc-1α*, we surgically removed the adrenal gland, and then stimulated VMHdm/c^{SF-1} neurons. Sham surgery were used as surgical controls. As we expected, the ADX eliminated blood corticosterone (Figure 2B). ADX mice were supplied with corticosterone in the drinking water to maintain the physiological levels of blood corticosterone (Figure 2C). We carried out optogenetic stimulation five days after ADX. ADX appeared not to affect Fos induction in the VMH (Figure 2D), suggesting ADX does not affect the ability of

254 VMHdm/c^{SF-1} neuronal activation. Indeed, plasma glucagon levels were significantly higher in
255 ADX mice after VMHdm/c^{SF-1} neuronal activation (Figure 2E). The removal of the adrenal
256 medulla in rats blocks hyperglycemia induced by microinjection of a cholinergic agonist into the
257 VMH[41]. In line with the report, VMHdm/c^{SF-1} neuronal activation could not increase blood
258 glucose levels in ADX mice at all (Figure 2F). Stunningly, ADX also completely blocked the
259 effects of VMHdm/c^{SF-1} neuronal activation on skeletal muscle *Pgc-1α* expression (Figure 2G),
260 suggesting that the sympathoadrenal drive, specifically the epinephrine release, is essential for
261 VMHdm/c^{SF-1} neuronal regulation of skeletal muscle function. In addition, these data suggest that
262 glucagon release unlikely contributes to VMHdm/c^{SF-1} neuronal-induced blood glucose levels.
263

264 **3.3 β2AdR is required for VMHdm/c^{SF-1} neuronal-induced skeletal muscle *Pgc-1α***

265 We assessed the contribution of β2AdR in VMHdm/c^{SF-1} neuronal-induced skeletal
266 muscle *Pgc-1α* expression. β2AdR is the major form of adrenergic receptors in skeletal muscle[42].
267 β2AdR agonist injection increases skeletal muscle *Pgc-1α-2, -3,* and *-4* mRNA levels[16],
268 suggesting that the sympathetic input coupled with β2AdR is key for skeletal muscle physiology.
269 We tested whether β2AdR global KO can diminish VMHdm/c^{SF-1} neuronal-induced skeletal
270 muscle *Pgc-1α* expression (Figure 3A). We first determined whether β2AdR KO affects the ability
271 of ChR2 to activate VMHdm/c^{SF-1} neurons. Optogenetic stimulation induced equal levels of Fos
272 expression in the VMH of wild-type and β2AdR KO mice (VMHdm/c^{SF-1}::ChR2-WT and
273 VMHdm/c^{SF-1}::ChR2-β2AdR^{KO}, Figure 3B), suggesting β2AdR KO does not affect the capacity
274 for optogenetic activation of VMHdm/c^{SF-1} neurons. Blood glucose and plasma glucagon in
275 VMHdm/c^{SF-1}::ChR2-β2AdR^{KO} were significantly higher than that of control group (VMHdm/c^{SF-}
276 ^{1}::mCherry-β2AdR^{KO}) (Figure 3C and D). In addition, optogenetic stimulation of VMHdm/c^{SF-1}

277 neurons significantly increased plasma epinephrine in β2AdR KO compared to non-stimulation
278 control (Figure 3E). VMHdm/c^{SF-1}::ChR2-β2AdR^{KO} showed significantly lower mRNA levels of
279 skeletal muscle *Pgc-1α-2, -3,* and *-4* compared to VMHdm/c^{SF-1}::ChR2-WT (Figure 3F).
280 Collectively, these results demonstrate that β2AdR is essential for VMHdm/c^{SF-1} neuronal-induced
281 skeletal muscle transcriptional regulation, but not blood glucose levels.
282

283 **3.4 Redundant functionality of downstream nodes of VMHdm/c^{SF-1} neurons**

284 VMHdm/c^{SF-1} neurons project to a broad range of the CNS sites that regulate the SNS
285 including presympathetic nodes[21]. Among these areas, we examined the contributions of the
286 aBNST, POA, AH, PVH/AH, and PAG to VMHdm/c^{SF-1} neuronal-induced augmentations in
287 plasma epinephrine, and skeletal muscle *Pgc-1α* expression. As the PVH and AH are located in
288 close proximity to each other (the AH is located at ventral side of the PVH), thus the light source
289 can reach to both areas based on the theoretical irradiance value calculation
290 (https://web.stanford.edu/group/dlab/cgi-bin/graph/chart.php), it is possible that the PVH
291 stimulation also affects the AH. Therefore, going forward, we will refer to optogenetic stimulation
292 in this region as the PVH/AH stimulation instead of the PVH stimulation. We injected AAV-DIO-
293 ChR2 into the VMH of *Sf-1* Cre mice followed by the insertion of the optic fiber probe into each
294 area (Figure 4A). Intriguingly, all terminal stimulations of VMHdm/c^{SF-1} neurons significantly
295 increased blood glucose (Figure 4B). While stimulation in each area also increased plasma
296 epinephrine (mean values ± SEM ; 1919 ± 324, 3869 ± 922, 3782 ± 594, 2759 ± 188, 5145 ± 841,
297 and 6311 ± 836 pg/mL for mCherry, aBNST, POA, AH, PVH/AH, and PAG, respectively), the
298 most striking differences were observed after terminal stimulation of VMHdm/c^{SF-1} neurons in the
299 PVH/AH and PAG (Figure 4C). We found that *Pgc-1α* total mRNA expression levels were

300 significantly increased in the terminal stimulation of the POA and PVH/AH (Figure 4D). *Pgc-1α-*
301 *1* mRNA expression levels were significantly increased in the terminal stimulation in the AH and
302 PVH/AH (Figure 4E). *Pgc-1α-2* and *-3* mRNA expression levels were significantly increased in
303 the terminal stimulation in the PVH/AH and PAG (Figure 4G). Finally, *Pgc-1α-4* mRNA
304 expression levels were significantly increased in the terminal stimulation in the PVH/AH. Of note,
305 although the terminal stimulation in the aBNST, POA, and AH did not statistically increase RNA
306 levels of skeletal muscle *Pgc-1α-2, -3,* and *-4*, the mean values were higher than those in the control
307 group. Collectively, we conclude that VMHdm/c^{SF-1} neuronal projections to the PVH/AH and PAG
308 have greater contributions to the regulation of skeletal muscle *Pgc-1α* mRNA expression and
309 plasma epinephrine. However, other projection sites likely contribute as well, indicating that
310 VMHdm/c^{SF-1} neurons use neurocircuits that are functionally redundant to regulate the
311 sympathoadrenal activity.

312 A previous study found that VMHdm/c^{SF-1} neurons project to downstream sites
313 collaterally[23]. For example, VMHdm/c^{SF-1} neurons projecting to the PAG also send axons to the
314 AH[40]. Each VMHdm/c^{SF-1} neuron likely projects to multiple sites, especially to the areas that
315 are topographically adjacent, such as aBNST and POA or the AH and PVH. In other words, when
316 the terminal activation of VMHdm/c^{SF-1} neurons at one downstream area occurs, back-propagated
317 neuronal activation could happen in other non-stimulated areas. To determine whether it is the
318 case, we assessed Fos expression after the terminal activation of VMHdm/c^{SF-1} neurons in the
319 aBNST, POA, AH, PVH/AH, and PAG as well as the soma stimulation of VMHdm/c^{SF-1} neurons
320 (Figure 5A and B). We compared the stimulated side (right hemisphere) and the non-stimulated
321 side (left hemisphere). As shown (Figure 1C), the optogenetic stimulation of the soma of
322 VMHdm/c^{SF-1} neurons (Figure 5O and P, S Figure 2E) significantly increased Fos expression in

323 the stimulated side of the VMH (Figure 5Q). Mice received the control AAV did not show any
324 difference between stimulated and non-stimulated sides after the VMH stimulation (S Figure 3).
325 Intriguingly, the soma activation of VMHdm/c^{SF-1} neurons significantly increased Fos expression
326 only in the PVH and AH (Figure 5Q). We did not find distal neuronal propagations by the terminal
327 activation in the POA, PVH/AH, AH, and PAG (Figure 5H, K, N, Q, and T, S Figure 2A, B, C, D
328 and F). The terminal stimulation in the aBNST increased Fos expression in distal site PAG (Figure
329 5E). However, it is unclear that Fos expression in the PAG was induced by the distal propagation
330 as Fos expression in the VMH was not changed after aBNST stimulation (Figure 5E). We
331 frequently observed Fos-expression in the sites proximal to the stimulated site. For instance, the
332 aBNST stimulation induced Fos-expression in the POA (Figure 5E). Likewise, the AH stimulation
333 induced Fos-expression in the PVH (Figure 5K), and the PVH/AH stimulation induced Fos-
334 expression in the POA and VMH (Figure 5N). Fos expression in the stimulated hemisphere of AH
335 was significantly higher of all the stimulation sites (Figure 5E, H, K, N, Q, and T), suggesting that
336 these Fos-inductions in the AH may be the secondary rather than direct propagated activation.

337 To further investigate the redundant roles of downstream sites of VMHdm/c^{SF-1} neurons
338 regulating the SNS, we stimulated the terminal of VMHdm/c^{SF-1} neurons in the PVH/AH or PAG
339 while suppressing the soma of VMHdm/c^{SF-1} neurons to eliminate back-propagations, at least,
340 between the PVH/AH and PAG. We selected these two sites as our data (Figure 4) showed that
341 stimulation of those two sites led to the most prominent the SNS activation. We confirmed that
342 Gi-DREADD hampers hyperglycemia, skeletal muscle *Pgc-1α* mRNA expression, and Fos
343 activation induced by optogenetics (S Figure 4). The terminal stimulation of PVH/AH or PAG still
344 induced hyperglycemia (S Figure 5A) and skeletal muscle *Pgc-1α* mRNA expression (S Figure 5B
345 and C) while Gi-DREADD inhibited VMHdm/c^{SF-1} neurons. However, Gi-DREADD significantly

346 suppressed *Pgc-1α* mRNA expression compared to control injection group (S Figure 5B and C).
347 Gi-DREADD suppressed Fos activation in the VMH by the terminal stimulation of PVH/AH or
348 PAG of VMHdm/c^{SF-1} neurons (S Figure 5D and F). As described above, we observed prominent
349 Fos activation in the AH by any conditions, further confirming that these Fos expression in the AH
350 may not be reflected to direct activation of VMHdm/c^{SF-1} neurons. The terminal stimulation of
351 PVH/AH with Gi-DREADD did not induce Fos in the PAG, while the terminal stimulation of PAG
352 with Gi-DREADD did not induce Fos in the VMH (S Figure 6 D and F). In these conditions, the
353 readouts of the SNS activity (glucose and skeletal *Pgc-1α* mRNA expression) were still increased
354 (S Figure 6A-C), suggesting that at least these two distal projection sites of VMHdm/c^{SF-1} neurons,
355 PVH/AH and PAG projections, are functionally redundant. Collectively, Fos expression data
356 indicated that each single VMHdm/c^{SF-1} neuronal axon projects many downstream sites
357 collaterally, strengthening the idea of functionally redundant VMHdm/c^{SF-1} neuronal circuits that
358 regulate the SNS.

359 **4.1 Discussion**

360 Here we demonstrate that VMHdm/c^{SF-1} neuronal circuits regulate skeletal muscle *Pgc-1α* mRNA
361 via the sympathoadrenal-released epinephrine coupled with β2AdR. Our data further predict that
362 VMHdm/c^{SF-1} neurons collaterally project multiple presympathetic nodes in the CNS that possess
363 redundant functions to regulate the sympathoadrenal activation. The VMH facilitates glucose
364 uptake in skeletal muscle and brown adipose tissue (BAT) and fatty acid mobilization from white
365 adipose tissues (WAT) by direct sympathetic innervation rather than the sympathoadrenal
366 drive[43-47]. Intriguingly, these studies have demonstrated that direct sympathetic innervation is
367 key for VMH-induced glucose uptake and lipolysis in BAT and skeletal muscle rather than the
368 sympathoadrenal activity[43; 44; 46; 47]. Contrary to these previous findings, results in this study
369 highlight the importance of the sympathoadrenal activity for VMHdm/c^{SF-1} neurons-induced
370 skeletal muscle *Pgc-1α* expression. Because VMH neurons are genetically heterogenous[48; 49],
371 it is possible that VMHdm/c^{SF-1} neurons regulate skeletal muscle function primarily via
372 sympathoadrenal activity, while other subtypes of neurons in the VMH mediate skeletal muscle
373 glucose uptake via the direct sympathetic innervation. Optogenetic activation of leptin receptors-
374 expressing neurons in the VMHdm/c does not affect blood glucose, plasma glucagon, and plasma
375 insulin levels[22], supporting the notion that functional segregation may exist within the
376 VMHdm/c neuronal subgroups. Further studies are warranted to reveal the mechanistic differences
377 among the genetically distinctive neuronal groups within the VMHdm/c that regulate skeletal
378 muscle function.

379 PGC-1α is one of the key molecules regulating a wide range of skeletal muscle
380 physiology[50]. PGC-1α-1 is "classic" PGC-1α, and regulates mitochondrial function, glucose and
381 fat metabolism[14; 39]. PGC-1α-4 regulates the protein synthesis[14; 39]. The physiological role

382 of PGC-1α-2 and -3 are still not clear. It is predicted that they contribute to angiogenesis, epithelial
383 function, chromosomal maintenance, and cholesterol metabolism[16]. PGC-1α-1 is derived from
384 the proximal promoter region of PGC-1α locus, and PGC-1α-2, -3, and -4 are derived from the
385 distal promoter region[10]. Intriguingly, running wheel activity and treadmill exercise activate the
386 distal promoter region but not the proximal promoter region[18; 51]. Furthermore, β2AdR agonist
387 also only initiates the transcription of PGC-1α exclusively at the proximal promoter region[18; 51],
388 leading to increased mRNA levels of PGC-1α-2, -3, and -4, but not PGC-1α-1[16]. These data
389 indicate the importance of the CNS→the SNS→skeletal muscle β2AdR axis for the regulation of
390 skeletal muscle PGC-1α in response to exercise. Our data demonstrate that VMHdm/c^{SF-1} neurons
391 can regulate PGC-1α-2, -3, and -4, but not -1, further strengthening the idea that these neurons are
392 important for exercise-induced augmentation of skeletal muscle function.

393 VMHdm/c^{SF-1} neuronal activation increases circulating epinephrine, and ADX completely
394 blocks VMHdm/c^{SF-1} neuronal-induced skeletal muscle *Pgc-1α* expression (Figure 2), suggesting
395 that epinephrine secretion from the adrenal grand is essential for VMHdm/c^{SF-1} neuronal regulation
396 of skeletal muscle function. Because the adrenal gland secretes many endocrine hormones, we
397 must consider the contribution of non-catecholamines hormones to VMHdm/c^{SF-1} neuronal-
398 induced skeletal muscle *Pgc-1α* expression. For instance, optogenetic activation of VMHdm/c^{SF-1}
399 neurons increases blood corticosterone[22]. Thus, it is possible that the surge of corticosterone
400 from the adrenal gland also contributes to VMHdm/c^{SF-1} neuronal-induced skeletal muscle *Pgc-*
401 *1α*. Corticosterone supplement (Figure 2B) can only provide physiologically stable corticosterone
402 levels but can not imitate endogenous dynamics of corticosterone releases. However,
403 dexamethasone (DEX) treatments suppress PGC-1α in skeletal muscle cell lines[52], and in the
404 testis of *in vivo* mouse model[53]. Glucocorticoid receptors (GRs) are expressed in skeletal muscle,

405 and skeletal muscle-specific GR-KO mice show increased lean mass[54], which is in line with the
406 fact that DEX can induce atrophy[55]. Therefore, we conclude that corticosterone unlikely
407 contributes to the induction of skeletal muscle PGC-1α after VMHdm/c^{SF-1} neuronal activation.
408 However, further studies are necessary to determine that epinephrine is the only factor in the
409 adrenal gland that contributes to VMHdm/c^{SF-1} neuronal-induced skeletal muscle *Pgc-1α*.

410 A large body of literature has concluded that β2AdR signaling is key to the regulation of
411 skeletal muscle PGC-1α expression[42], and ultimately orchestrating protein
412 synthesis/degradation, glucose and fat metabolism, and angiogenesis[9; 10; 51]. Our study extends
413 these findings to show that the sympathoadrenal activity coupled with β2AdR is essential for
414 VMHdm/c^{SF-1} neuronal-induced skeletal muscle *Pgc-1α* expression (Figure 3). β2AdR is
415 expressed throughout the body[18], and even within the skeletal muscle, β2AdR is expressed in a
416 variety of cell types including skeletal muscle cells, smooth muscle cells (blood vessels), and
417 endothelial cells[42; 56]. In addition, recent studies highlight the key role of β2AdR at the
418 neuromuscular junctions (NMJs) to regulate acetylcholine and acetylcholine receptors[57; 58]. As
419 we used global β2 AdR KO mice, we can not formally exclude the possibility that β2AdR in the
420 non-skeletal muscle organs are actually essential. Further studies using tissue specific β2AdR
421 manipulation (e.g., deletion of β2AdR in specifically skeletal or smooth muscle cells) are
422 necessary to decipher the precise targets of VMHdm/c^{SF-1} neurons and the sympathoadrenal axis.

423 The terminal activation of VMHdm/c^{SF-1} neurons in the PVH/AH and PAG significantly
424 increases blood epinephrine and skeletal muscle *Pgc-1α-2 and -3* mRNA (Figure 4). Because the
425 PVH and PAG directly project to the sympathoadrenal preganglionic neurons in the
426 intermediolateral nucleus of the spinal cord[59-62], it is predicted that activation of these areas can
427 have more profound effects on the sympathoadrenal activity. By comparing the results of the

428 PVH/AH and AH stimulation (Figure 4), it is likely that VMHdm/c^{SF-1} neurons projecting to the
429 PVH substantially contribute to the regulation of the SNS activity than that to the AH. Because
430 ADX completely diminishes augmented blood glucose by VMHdm/c^{SF-1} neuronal stimulation
431 (Figure 2), epinephrine release by the SNS activation is likely required for the augmented blood
432 glucose levels. Interestingly, the terminal activation in all sites we investigated significantly
433 increased blood glucose (Figure 4). Taken together, blood glucose data (Figure 4) indicate that all
434 sites we investigated can activate the sympathoadrenal activity, although the degree of the
435 sympathoadrenal activation may vary. In fact, the mean value of blood epinephrine, skeletal
436 muscle *Pgc-1* mRNA levels in all the sites are higher than control group (Figure 4), suggesting
437 that all sites we investigated contribute to VMHdm/c^{SF-1}-neuronal regulation of the
438 sympathoadrenal activity at some extent of degree. Collectively, these data suggest that the
439 downstream sites of VMHdm/c^{SF-1} neurons have redundant functions regarding the augmented
440 sympathoadrenal activity.

441 The Fos expression data (Figure 5) indicate that VMHdm/c^{SF-1} neuronal axon projections
442 are collaterals rather than one-to-one projections[63] as terminal stimulations can induce back-
443 propagated activation in the proximal projected sites of VMHdm/c^{SF-1} neuronal (Figure 5). A
444 previous study using the retrograde tracing method supports this notion as they found that most of
445 VMHdm/c^{SF-1} neurons project to the AH also collaterally send the axon to the PAG[23]. The VMH
446 regulate essential physiological function for survival and high-energy demand situations including
447 counterregulatory actions to hypoglycemia[3], defensive behavior[23; 40], and exercise[5; 64].
448 These survival functions have to be executed coordinately at the whole-body level. Considering
449 that collateral VMHdm/c^{SF-1} neuronal circuits are functionally redundant, we propose that similar
450 to monoaminergic neurons[65], VMHdm/c^{SF-1} neurons play a “broadcast” role in the regulation of

451 physiological functions at the whole-body level during emergency or high-energy demand
452 situations. Further studies will be necessary to delineate the degree of contributions of each
453 VMHdm/c^{SF-1} neuronal downstream node to the regulation of metabolism.
454

455 **4.2 Limitation of this study**

456 As many previous studies have noted, optogenetic stimulation induces firing patterns that
457 are dissimilar to endogenous firing patterns in many neurons[66]. Therefore, we can not exclude
458 the possibility that our data demonstrate the maximum capability of VMHdm/c^{SF-1} neurons on the
459 regulation of skeletal muscle rather physiological roles of VMHdm/c^{SF-1} neurons. We also used a
460 fixed optogenetic configuration throughout the terminal activations, despite the fact that each site
461 we investigated has a different density of VMHdm/c^{SF-1} neuronal axon and terminals[21]. It is
462 virtually possible that different terminal sites require different firing pattern to execute their
463 function properly. Future studies to use fine-tuning configuration are necessary to test this
464 possibility.

465 As we mentioned above, the inherent limitations of the ADX studies have to be considered.
466 Although we supplied the corticosterone to maintain its physiological levels, the surgical removal
467 of the adrenal gland can compromise many physiological functions directly and indirectly. For
468 instance, we observed that the basal levels of skeletal muscle *Pgc-1α* were decreased in ADX mice
469 (56%, 51%, 96%, 95%, and 72% mean reductions in *Pgc-1α total, Pgc-1α-1, Pgc-1α-2, Pgc-1α-3,*
470 *and Pgc-1α-4* respectively compared to sham control, in Figure 2G). To exclude the possibility
471 that ADX affects the sensitivity of adrenergic receptors, we investigated whether β2AdR agonist
472 can induce skeletal muscle *Pgc-1α* in ADX mice. β2AdR agonist significantly induced skeletal
473 muscle *Pgc-1α*, and there were no significant differences between sham and ADX mice (SFigure

474 6). Thus, ADX unlikely affects the sensitivity of adrenergic receptors in skeletal muscle in our
475 experimental design. Nonetheless, we have to interpret ADX studies with careful consideration,
476 and future experiments using sophisticated techniques (e.g., genetic-ablation of epinephrine only
477 from the adrenal medulla) will be warranted to further confirm the role of epinephrine releases
478 from the adrenal medulla in the regulation of skeletal muscle physiology.

479 Fos protein expression is used as the readout of neuronal activity. However, there are
480 limitations we have to consider. First, we can not distinguish whether Fos activation is direct
481 consequences of VMHdm/c^{SF-1} neuronal activation or indirect consequences of physiological
482 changes induced by VMHdm/c^{SF-1} neuronal activation. For instance, it is well appreciated that
483 stressors can increase Fos expressions. VMHdm/c^{SF-1} neuronal activation clearly induce fight or
484 flight type of endocrine responses (e.g., increased epinephrine, corticosterone, glucagon, and
485 glucose in the blood), that potentially can increase Fos expression indirectly.

486

487 **4.3 Conclusion**

488 The CNS-skeletal muscle interactions are important to maintain metabolic homeostasis.
489 The skeletal muscle plays a critical role in the regulation of metabolic homeostasis as it
490 substantially contributes to basal energy expenditure and glucose disposal after meal[13; 67]. A
491 large body of studies has built the foundation of neuroanatomy regarding metabolic
492 homeostasis[62]. In the last decade**,** optogenetic tools have revealed detailed functional
493 neurocircuits regulating metabolism including food intake and glucose metabolism[1; 68; 69]. This
494 study using optogenetics demonstrates that VMHdm/c^{SF-1} neurons regulate skeletal muscle PGC1-
495 α via epinephrine released from the adrenal gland coupled with β2AdR. In addition, our data
496 suggest that VMHdm/c^{SF-1} neuronal circuits regulating the sympathoadrenal activity are

497 functionally redundant, yet varied contributions from each downstream node to the regulation of
498 the SNS likely exist (SFigure 7). Our study advances the understanding of brain-skeletal muscle
499 communications and implies the significant contributions of VMHdm/c^{SF-1}
500 neurons→sympathoadrenal axis to beneficial effects of exercise on skeletal muscle.

5. Acknowledgement

We thank Glenn Toney at UT Health San Antonio (UTHSA) for valuable advice, Nancy Gonzalez and Harun A. Khan (UTHSA), Bandy Chen, Safia Baset, and Jasmine Dushime (UTSW) for the technical assistant, Juri C. Fujikawa for providing animal illustrations, and Steven Wyler, Ryan Reynolds, Luis Leon Mercado, Syann Lee, and Joel. K. Elmquist (UTSW) for valuable comments on the manuscript. This work was supported by the University of Texas System (UT Rising STARs to T.F.), and San Antonio Area Foundation (to T.F.). This manuscript has been released as a pre-print at Biorxiv (https://www.biorxiv.org/content/10.1101/2022.04.01.486756v1).

6. Competing interests

The authors do not have any conflict of interest.

7. Contribution

T.Y. designed, performed and analyzed experiments, and edited the manuscript. M. F., S.F., A.H., Z.S., J.L., A.S.T., and A.K.S., performed experiments. T.F. designed, performed, supervised, and analyzed experiments, and wrote and finalized the manuscript.

517 **Figure Legends**

518 **Figure 1. Optogenetic activation of VMHdm/c^{SF-1} neurons increases mRNA levels of skeletal**
519 **muscle *Pgc1-α*** (**A**) Schematic figure of targeting site of VMHdm/c^{SF-1} neurons. (**B**) Experimental
520 design and stimulus setting of optogenetics. (**C**) Representative figures of Fos expression pattern
521 in the hypothalamus of mice expressing ChR2 in SF-1 expression neurons in VMHdm/c
522 (VMHdm/c^{SF-1}::ChR2) after VMHdm/c^{SF-1} neurons stimulation. (**D**) Blood glucose, (**E**) plasma
523 glucagon, (**F**) plasma insulin in mice after VMHdm/c^{SF-1} neuronal stimulation. Control group is
524 composed of mice expressing mCherry in VMHdm/c^{SF-1} neurons (VMHdm/c^{SF-1}::mCherry) (**G**)
525 mRNA expression levels of *Pgc1-α* isoform in skeletal muscle of VMHdm/c^{SF-1}::ChR2 mice after
526 optogenetic stimulation. (**H**) Plasma norepinephrine and (**I**) epinephrine in VMHdm/c^{SF-1}::ChR2
527 mice after optogenetic stimulation. Values are mean ± S.E.M. *** $p < 0.001$, * $p < 0.05$.

528

529 **Figure 2. Adrenalectomy (ADX) completely blocks VMHdm/c^{SF-1} neurons-induced blood**
530 **glucose and skeletal muscle *Pgc1-α* expression** (**A**) Schematic of ADX experimental design. (**B**)
531 Blood corticosterone levels before and after ADX in mice. (**C**) Blood corticosterone levels in ADX
532 mice with and without corticosterone supplementation. (**D**) Representative figures of Fos
533 expression pattern in the hypothalamus of ADX mice expressing ChR2 in SF-1 expression neurons
534 in VMHdm/c (VMHdm/c^{SF-1}::ChR2-ADX) and the number of Fos positive cells in the VMH of
535 VMHdm/c^{SF-1}::ChR2-ADX and sham VMHdm/c^{SF-1}::ChR2 (VMHdm/c^{SF-1}::ChR2-sham). (**E**)
536 Blood glucose, (**F**) plasma glucagon, and (**G**) mRNA expression levels of *Pgc1-α* isoform in
537 skeletal muscle of VMHdm/c^{SF-1}::ChR2-ADX after optogenetic stimulation. Values are mean ±
538 S.E.M. **** $p < 0.0001$, *** $p < 0.001$, ** $p < 0.01$, * $p < 0.05$.

539

540 **Figure 3. Ablation of β2AdR hampers VMHdm/c^{SF-1} neurons-induced skeletal muscle *Pgc1-α*** (**A**) Schematic of experimental design. (**B**) Representative figures of Fos expression pattern in
541
542 the hypothalamus of VMHdm/c^{SF-1}::ChR2 mice lacking β2AdR (VMHdm/c^{SF-1}::ChR2-β2AdR^{KO}),
543 and the number of Fos positive cells in the VMH of VMHdm/c^{SF-1}::ChR2- β2AdR^{KO} and wild-
544 type control (WT) (VMHdm/c^{SF-1}::ChR2-WT). (**C**) Blood glucose and (**D**) plasma glucagon levels
545 in VMHdm/c^{SF-1}::ChR2-β2AdR^{KO} mice after optogenetic stimulation. (**E**) Plasma epinephrine
546 levels in VMHdm/c^{SF-1}::ChR2-β2AdR^{KO} mice with and without optogenetic stimulation. (**F**)
547 mRNA expression levels of *Pgc1-α* isoform in skeletal muscle of ChR2- β2AdR^{KO} mice after
548 optogenetic stimulation. Values are mean ± S.E.M. **** $p < 0.0001$, ** $p < 0.01$, * $p < 0.05$.
549

550 **Figure 4. Downstream nodes of VMHdm/c^{SF-1} neurons are functionally redundant to**
551 **regulate the sympathoadrenal activity**. (**A**) Schematic figure of experimental design. (**B**) Blood
552 glucose levels in VMHdm/c^{SF-1}::ChR2 mice before and after the terminal stimulation of the
553 anterior bed nucleus of the stria terminalis (aBNST), preoptic area (POA), anterior hypothalamus
554 area (AH), paraventricular hypothalamic nucleus (PVH) and AH, and periaqueductal gray (PAG).
555 Control group is VMHdm/c^{SF-1}::mCherry mice after the VMH stimulation. (**C**) Plasma epinephrine
556 levels in VMHdm/c^{SF-1}::ChR2 mice after the terminal stimulation of aBNST, POA, AH, PVH/AH,
557 and PAG. (**D**) mRNA expression levels of *Pgc1-α-Total*, (**E**) *Pgc1-α-1*, (**F**) *Pgc1-α-2*, (**G**) *Pgc1-*
558 *α-3*, and (**H**) *Pgc1-α-4*, skeletal muscle of VMHdm/c^{SF-1}::ChR2 mice after the terminal stimulation
559 of aBNST, POA, AH, PVH/AH, and PAG. Values are mean ± S.E.M. **** $p < 0.0001$, *** $p <$
560 0.001, ** $p < 0.01$, * $p < 0.05$.
561

562 **Figure 5. The terminal activation of VMHdm/c^{SF-1} neurons evokes Fos expression in the**
563 **proximal terminal sites**. (**A**) Schematic figure of experimental design. (**B**) Schematic of Fos
564 expression counts in the nucleus. The brain maps of optic fiber insertion sites of (**C**), aBNST, (**F**)
565 POA (**I**), AH (**L**), PVH/AH, (**O**), VMH, and (**R**) PAG. Representative figures of Fos expression
566 at the terminal sites or soma of VMHdm/c^{SF-1} neurons; (**D**) aBNST, (**G**) POA, (**J**) AH, (**M**)
567 PVH/AH, (**P**), VMHdm/c, and (**S**) PAG. The number of Fos expression cells at the aBNST, POA,
568 AH, PVH/AH, and PAG of VMHdm/c^{SF-1}::ChR2 mice after the terminal stimulation of (**E**) aBNST,
569 (**H**) POA, (**K**) AH, (**N**) PVH/AH, (**Q**) VMHdm/c and (**T**) PAG. Values are mean ± S.E.M. ****
570 $p < 0.0001$, *** $p < 0.001$, ** $p < 0.01$, * $p < 0.05$.
571

572 **Supplemental Figure 1, related to Figure 1.** mRNA expression levels of *Pgc1-α* isoform in
573 skeletal muscle of VMHdm/c^{SF-1}::ChR2 mice exhibiting freeze or burst behavior after optogenetic
574 stimulation. The stimulation configuration was the same as described in Figure 1. Freeze group
575 was composed of mice that only exhibited freeze behavior. Burst group was composed of mice
576 exhibited burst activity with or without other behavioral changes such as freeze behavior. Values
577 are mean ± S.E.M., *** $p < 0.001$, * $p < 0.05$.
578
579 **Supplemental Figure 2, related to Figure 5.** The high-resolution brain maps of optic fiber
580 insertion sites of (**A**), aBNST, (**B**) POA (**C**), AH (**D**), PVH/AH, (**E**), VMH, and (**F**) PAG.
581
582 **Supplemental Figure 3, related to Figure 5.** (**A**) Representative figure of the VMH, and (**B**) the
583 number of Fos expression cells at the aBNST, POA, AH, PVH/AH, and PAG of VMHdm/c^{SF-}
584 ^{1}::mCherry mice after the soma stimulation of VMH.
585
586 **Supplemental Figure 4, related to Figure 5.** (**A**) Schematic of experimental design. (**B**) Blood
587 glucose levels of Before (0 minutes) and 30 minutes after the VMH stimulation VMHdm/c^{SF-}
588 ^{1}::ChR2::Gi-DREADD mice. CNO (2.5 mg/kg) was i.p. injected 10 minutes before after the VMH
589 stimulation. Saline was used as control for CNO. (**C**) mRNA expression levels of *Pgc1 isoforms*
590 in skeletal muscle of VMHdm/c^{SF-1}::ChR2::Gi-DREADD mice after the terminal stimulation while
591 CNO (2.5 mg/kg) was i.p. injected. Control mice were VMHdm/c^{SF-1}::EYFP::Gi-DREADD mice
592 with the VMH stimulation. Representative figures of Fos expression the VMH in VMHdm/c^{SF-}
593 ^{1}::ChR2::Gi-DREADD mice after the terminal stimulation while (**D**) saline or (**E**) CNO (2.5
594 mg/kg) was i.p. injected. Magenta, Red, Green, and Blue represents Fos expression, Gi-DREADD,

595 ChR2, and DAPI, respectively. (**F**) Fos number in the VMH in VMHdm/c^{SF-1}::ChR2::Gi-
596 DREADD mice after the terminal stimulation while saline or CNO (2.5 mg/kg) was i.p. injected.
597 The stimulation setting was 5 ms duration, 10 Hz, 2 seconds activation and 2 seconds rest cycle,
598 30 minutes. Values are mean ± S.E.M. ** $p < 0.01$, * $p < 0.05$.
599
600 **Supplemental Figure 5, related to Figure 5.** (**A**) Blood glucose levels before (0 minutes) and 30
601 minutes after the terminal stimulation of VMHdm/c^{SF-1} neurons at the PVH/AH or PAG in
602 VMHdm/c^{SF-1}::ChR2::Gi-DREADD mice. CNO (2.5 mg/kg) was i.p. injected 10 minutes before
603 after the terminal stimulation. Saline was used as control for CNO. Control mice for Gi-DREADD
604 were administered rAAV5-EF1α-DIO-EYFP with rAAV8-hSyn-DIO-hM4D(Gi)-mCherry into
605 the VMH of *Sf-1*-BAC-Cre mice. mRNA expression levels of *Pgc1 isoforms* in skeletal muscle of
606 VMHdm/c^{SF-1}::ChR2::Gi-DREADD mice after the terminal stimulation of VMHdm/c^{SF-1} neurons
607 at the (**B**) PVH/AH or (**C**) PAG while CNO (2.5 mg/kg) was i.p. injected. Control mice were
608 VMHdm/c^{SF-1}::EYFP::Gi-DREADD mice with the VMH stimulation. Fos number in the PVH,
609 AH, VMH, and PAG in VMHdm/c^{SF-1}::ChR2::Gi-DREADD mice after the terminal stimulation
610 at the (**D**) PVH/AH or (**E**) PAG while saline or CNO (2.5 mg/kg) was i.p. injected. The stimulation
611 setting was 5 ms duration, 10 Hz (PVH/AH) or 20 Hz (PAG), 2 seconds activation and 2 seconds
612 rest cycle, 30 minutes. Values are mean ± S.E.M. **** $p < 0.0001$, *** $p < 0.001$, ** $p < 0.01$, * p
613 < 0.05.
614
615 **Supplemental Figure 6, related to Figure 2.** mRNA expression levels of *Pgc1-α* isoform in
616 skeletal muscle of ADX mice after β2AdR agonist (clenbuterol 1 mg per kg bodyweight, dissolved
617 in sterile saline solution). Values are mean ± S.E.M. *** $p < 0.001$, ** $p < 0.01$, * $p < 0.05$.

618

619 **Supplemental Figure 7.** Summary figure depicting pathways by which VMHdm/c^{SF-1} neurons

620 regulate skeletal muscle *Pgc1-α* expression and blood glucose levels via the sympathoadrenal

621 gland.

References

[1] Gautron, L., Elmquist, J.K., Williams, K.W., 2015. Neural control of energy balance: translating circuits to therapies. Cell 161(1):133-145.

[2] Morton, G.J., Meek, T.H., Schwartz, M.W., 2014. Neurobiology of food intake in health and disease. Nat Rev Neurosci 15(6):367-378.

[3] Stanley, S., Moheet, A., Seaquist, E.R., 2019. Central Mechanisms of Glucose Sensing and Counterregulation in Defense of Hypoglycemia. Endocr Rev 40(3):768-788.

[4] Zhang, Z., Boelen, A., Kalsbeek, A., Fliers, E., 2018. TRH Neurons and Thyroid Hormone Coordinate the Hypothalamic Response to Cold. Eur Thyroid J 7(6):279-288.

[5] Fujikawa, T., Castorena, C.M., Lee, S., Elmquist, J.K., 2017. The hypothalamic regulation of metabolic adaptations to exercise. J Neuroendocrinol 29(10).

[6] Fujikawa, T., Castorena, C.M., Pearson, M., Kusminski, C.M., Ahmed, N., Battiprolu, P.K., et al., 2016. SF-1 expression in the hypothalamus is required for beneficial metabolic effects of exercise. Elife 5.

[7] Zhao, L., Bakke, M., Krimkevich, Y., Cushman, L.J., Parlow, A.F., Camper, S.A., et al., 2001. Steroidogenic factor 1 (SF1) is essential for pituitary gonadotrope function. Development 128(2):147-154.

[8] Parker, K.L., Rice, D.A., Lala, D.S., Ikeda, Y., Luo, X., Wong, M., et al., 2002. Steroidogenic factor 1: an essential mediator of endocrine development. Recent Prog Horm Res 57:19-36.

[9] Handschin, C., Spiegelman, B.M., 2008. The role of exercise and PGC1alpha in inflammation and chronic disease. Nature 454(7203):463-469.

[10] Ruas, J.L., White, J.P., Rao, R.R., Kleiner, S., Brannan, K.T., Harrison, B.C., et al., 2012. A PGC-1alpha isoform induced by resistance training regulates skeletal muscle hypertrophy. Cell 151(6):1319-1331.

[11] Handschin, C., Choi, C.S., Chin, S., Kim, S., Kawamori, D., Kurpad, A.J., et al., 2007. Abnormal glucose homeostasis in skeletal muscle-specific PGC-1alpha knockout mice reveals skeletal muscle-pancreatic beta cell crosstalk. J Clin Invest 117(11):3463-3474.

[12] Benton, C.R., Nickerson, J.G., Lally, J., Han, X.X., Holloway, G.P., Glatz, J.F., et al., 2008. Modest PGC-1alpha overexpression in muscle in vivo is sufficient to increase insulin sensitivity and palmitate oxidation in subsarcolemmal, not intermyofibrillar, mitochondria. J Biol Chem 283(7):4228-4240.

[13] Hawley, J.A., Hargreaves, M., Joyner, M.J., Zierath, J.R., 2014. Integrative biology of exercise. Cell 159(4):738-749.

[14] Kang, C., Li Ji, L., 2012. Role of PGC-1alpha signaling in skeletal muscle health and disease. Ann N Y Acad Sci 1271:110-117.

[15] Barres, R., Yan, J., Egan, B., Treebak, J.T., Rasmussen, M., Fritz, T., et al., 2012. Acute exercise remodels promoter methylation in human skeletal muscle. Cell Metab 15(3):405-411.

[16] Martinez-Redondo, V., Jannig, P.R., Correia, J.C., Ferreira, D.M., Cervenka, I., Lindvall, J.M., et al., 2016. Peroxisome Proliferator-activated Receptor gamma Coactivator-1 alpha Isoforms Selectively Regulate Multiple Splicing Events on Target Genes. J Biol Chem 291(29):15169-15184.

[17] Miura, S., Kawanaka, K., Kai, Y., Tamura, M., Goto, M., Shiuchi, T., et al., 2007. An increase in murine skeletal muscle peroxisome proliferator-activated receptor-gamma coactivator-

1alpha (PGC-1alpha) mRNA in response to exercise is mediated by beta-adrenergic receptor activation. Endocrinology 148(7):3441-3448.
[18] Miura, S., Kai, Y., Kamei, Y., Ezaki, O., 2008. Isoform-specific increases in murine skeletal muscle peroxisome proliferator-activated receptor-gamma coactivator-1alpha (PGC-1alpha) mRNA in response to beta2-adrenergic receptor activation and exercise. Endocrinology 149(9):4527-4533.
[19] Uyama, N., Geerts, A., Reynaert, H., 2004. Neural connections between the hypothalamus and the liver. Anat Rec A Discov Mol Cell Evol Biol 280(1):808-820.
[20] Shimazu, T., Minokoshi, Y., 2017. Systemic Glucoregulation by Glucose-Sensing Neurons in the Ventromedial Hypothalamic Nucleus (VMH). J Endocr Soc 1(5):449-459.
[21] Lindberg, D., Chen, P., Li, C., 2013. Conditional viral tracing reveals that steroidogenic factor 1-positive neurons of the dorsomedial subdivision of the ventromedial hypothalamus project to autonomic centers of the hypothalamus and hindbrain. J Comp Neurol 521(14):3167-3190.
[22] Meek, T.H., Nelson, J.T., Matsen, M.E., Dorfman, M.D., Guyenet, S.J., Damian, V., et al., 2016. Functional identification of a neurocircuit regulating blood glucose. Proc Natl Acad Sci U S A.
[23] Wang, L., Chen, I.Z., Lin, D., 2015. Collateral pathways from the ventromedial hypothalamus mediate defensive behaviors. Neuron 85(6):1344-1358.
[24] Zhang, J., Chen, D., Sweeney, P., Yang, Y., 2020. An excitatory ventromedial hypothalamus to paraventricular thalamus circuit that suppresses food intake. Nat Commun 11(1):6326.
[25] Bachman, E.S., Dhillon, H., Zhang, C.Y., Cinti, S., Bianco, A.C., Kobilka, B.K., et al., 2002. betaAR signaling required for diet-induced thermogenesis and obesity resistance. Science 297(5582):843-845.
[26] Fujikawa, T., Berglund, E.D., Patel, V.R., Ramadori, G., Vianna, C.R., Vong, L., et al., 2013. Leptin engages a hypothalamic neurocircuitry to permit survival in the absence of insulin. Cell Metab 18(3):431-444.
[27] Singha, A., Palavicini, J.P., Pan, M., Farmer, S., Sandoval, D., Han, X., et al., 2020. Leptin Receptors in RIP-Cre(25Mgn) Neurons Mediate Anti-dyslipidemia Effects of Leptin in Insulin-Deficient Mice. Front Endocrinol (Lausanne) 11:588447.
[28] Keith B. J. Franklin, G.P., 2008. The Mouse Brain in Stereotaxic Coordinates. Academic Press.
[29] Singha, A.K., Yamaguchi, J., Gonzalez, N.S., Ahmed, N., Toney, G.M., Fujikawa, T., 2019. Glucose-Lowering by Leptin in the Absence of Insulin Does Not Fully Rely on the Central Melanocortin System in Male Mice. Endocrinology 160(3):651-663.
[30] Fujikawa, T., Chuang, J.C., Sakata, I., Ramadori, G., Coppari, R., 2010. Leptin therapy improves insulin-deficient type 1 diabetes by CNS-dependent mechanisms in mice. Proc Natl Acad Sci U S A 107(40):17391-17396.
[31] Miyaki, T., Fujikawa, T., Kitaoka, R., Hirano, N., Matsumura, S., Fushiki, T., et al., 2011. Noradrenergic projections to the ventromedial hypothalamus regulate fat metabolism during endurance exercise. Neuroscience 190:239-250.
[32] Asterholm, I.W., Rutkowski, J.M., Fujikawa, T., Cho, Y.R., Fukuda, M., Tao, C., et al., 2014. Elevated resistin levels induce central leptin resistance and increased atherosclerotic progression in mice. Diabetologia 57(6):1209-1218.

[33] Williams, K.W., Liu, T., Kong, X., Fukuda, M., Deng, Y., Berglund, E.D., et al., 2014. Xbp1s in Pomc Neurons Connects ER Stress with Energy Balance and Glucose Homeostasis. Cell Metab 20(3):471-482.
[34] Castorena, C.M., Caron, A., Michael, N.J., Ahmed, N.I., Arnold, A.G., Lee, J., et al., 2021. CB1Rs in VMH neurons regulate glucose homeostasis but not body weight. Am J Physiol Endocrinol Metab 321(1):E146-E155.
[35] Berndt, A., Schoenenberger, P., Mattis, J., Tye, K.M., Deisseroth, K., Hegemann, P., et al., 2011. High-efficiency channelrhodopsins for fast neuronal stimulation at low light levels. Proc Natl Acad Sci U S A 108(18):7595-7600.
[36] Dhillon, H., Zigman, J.M., Ye, C., Lee, C.E., McGovern, R.A., Tang, V., et al., 2006. Leptin directly activates SF1 neurons in the VMH, and this action by leptin is required for normal body-weight homeostasis. Neuron 49(2):191-203.
[37] Shimazu, T., Fukuda, A., Ban, T., 1966. Reciprocal influences of the ventromedial and lateral hypothalamic nuclei on blood glucose level and liver glycogen content. Nature 210(5041):1178-1179.
[38] Flak, J.N., Goforth, P.B., Dell'Orco, J., Sabatini, P.V., Li, C., Bozadjieva, N., et al., 2020. Ventromedial hypothalamic nucleus neuronal subset regulates blood glucose independently of insulin. J Clin Invest 130(6):2943-2952.
[39] Martinez-Redondo, V., Pettersson, A.T., Ruas, J.L., 2015. The hitchhiker's guide to PGC-1alpha isoform structure and biological functions. Diabetologia 58(9):1969-1977.
[40] Kunwar, P.S., Zelikowsky, M., Remedios, R., Cai, H., Yilmaz, M., Meister, M., et al., 2015. Ventromedial hypothalamic neurons control a defensive emotion state. Elife 4.
[41] Brito, N.A., Brito, M.N., Kettelhut, I.C., Migliorini, R.H., 1993. Intra-ventromedial hypothalamic injection of cholinergic agents induces rapid hyperglycemia, hyperlactatemia and gluconeogenesis activation in fed, conscious rats. Brain Res 626(1-2):339-342.
[42] Lynch, G.S., Ryall, J.G., 2008. Role of beta-adrenoceptor signaling in skeletal muscle: implications for muscle wasting and disease. Physiol Rev 88(2):729-767.
[43] Takahashi, A., Shimazu, T., 1981. Hypothalamic regulation of lipid metabolism in the rat: effect of hypothalamic stimulation on lipolysis. Journal of the autonomic nervous system 4(3):195-205.
[44] Minokoshi, Y., Saito, M., Shimazu, T., 1986. Sympathetic denervation impairs responses of brown adipose tissue to VMH stimulation. Am J Physiol 251(5 Pt 2):R1005-1008.
[45] Sudo, M., Minokoshi, Y., Shimazu, T., 1991. Ventromedial hypothalamic stimulation enhances peripheral glucose uptake in anesthetized rats. The American journal of physiology 261(3 Pt 1):E298-303.
[46] Haque, M.S., Minokoshi, Y., Hamai, M., Iwai, M., Horiuchi, M., Shimazu, T., 1999. Role of the sympathetic nervous system and insulin in enhancing glucose uptake in peripheral tissues after intrahypothalamic injection of leptin in rats. Diabetes 48:1706-1712.
[47] Minokoshi, Y., Haque, M.S., Shimazu, T., 1999. Microinjection of leptin into the ventromedial hypothalamus increases glucose uptake in peripheral tissues in rats. Diabetes 48(2):287-291.
[48] Affinati, A.H., Sabatini, P.V., True, C., Tomlinson, A.J., Kirigiti, M., Lindsley, S.R., et al., 2021. Cross-species analysis defines the conservation of anatomically segregated VMH neuron populations. Elife 10.

[49] van Veen, J.E., Kammel, L.G., Bunda, P.C., Shum, M., Reid, M.S., Massa, M.G., et al., 2020. Hypothalamic estrogen receptor alpha establishes a sexually dimorphic regulatory node of energy expenditure. Nat Metab 2(4):351-363.
[50] Lira, V.A., Benton, C.R., Yan, Z., Bonen, A., 2010. PGC-1alpha regulation by exercise training and its influences on muscle function and insulin sensitivity. Am J Physiol Endocrinol Metab 299(2):E145-161.
[51] Chinsomboon, J., Ruas, J., Gupta, R.K., Thom, R., Shoag, J., Rowe, G.C., et al., 2009. The transcriptional coactivator PGC-1alpha mediates exercise-induced angiogenesis in skeletal muscle. Proc Natl Acad Sci U S A 106(50):21401-21406.
[52] Rahnert, J.A., Zheng, B., Hudson, M.B., Woodworth-Hobbs, M.E., Price, S.R., 2016. Glucocorticoids Alter CRTC-CREB Signaling in Muscle Cells: Impact on PGC-1alpha Expression and Atrophy Markers. PLoS One 11(7):e0159181.
[53] Annie, L., Gurusubramanian, G., Kumar Roy, V., 2019. Dexamethasone mediated downregulation of PGC-1alpha and visfatin regulates testosterone synthesis and antioxidant system in mouse testis. Acta Histochem 121(2):182-188.
[54] Shimizu, N., Maruyama, T., Yoshikawa, N., Matsumiya, R., Ma, Y., Ito, N., et al., 2015. A muscle-liver-fat signalling axis is essential for central control of adaptive adipose remodelling. Nat Commun 6:6693.
[55] Pereira, R.M., Freire de Carvalho, J., 2011. Glucocorticoid-induced myopathy. Joint Bone Spine 78(1):41-44.
[56] Conti, V., Russomanno, G., Corbi, G., Izzo, V., Vecchione, C., Filippelli, A., 2013. Adrenoreceptors and nitric oxide in the cardiovascular system. Front Physiol 4:321.
[57] Khan, M.M., Lustrino, D., Silveira, W.A., Wild, F., Straka, T., Issop, Y., et al., 2016. Sympathetic innervation controls homeostasis of neuromuscular junctions in health and disease. Proc Natl Acad Sci U S A 113(3):746-750.
[58] Rodrigues, A.C.Z., Messi, M.L., Wang, Z.M., Abba, M.C., Pereyra, A., Birbrair, A., et al., 2019. The sympathetic nervous system regulates skeletal muscle motor innervation and acetylcholine receptor stability. Acta Physiol (Oxf) 225(3):e13195.
[59] Strack, A.M., Sawyer, W.B., Platt, K.B., Loewy, A.D., 1989. CNS cell groups regulating the sympathetic outflow to adrenal gland as revealed by transneuronal cell body labeling with pseudorabies virus. Brain Res 491(2):274-296.
[60] Jansen, A.S., Nguyen, X.V., Karpitskiy, V., Mettenleiter, T.C., Loewy, A.D., 1995. Central command neurons of the sympathetic nervous system: basis of the fight-or-flight response. Science 270(5236):644-646.
[61] Saper, C.B., Loewy, A.D., Swanson, L.W., Cowan, W.M., 1976. Direct hypothalamo-autonomic connections. Brain Res 117(2):305-312.
[62] Saper, C.B., Stornetta, R.L., 2015. The Rat Nervous System, 4th Edition, Chapter 23. Academic Press:629-673.
[63] Betley, J.N., Cao, Z.F., Ritola, K.D., Sternson, S.M., 2013. Parallel, redundant circuit organization for homeostatic control of feeding behavior. Cell 155(6):1337-1350.
[64] Cavalcanti-de-Albuquerque, J.P., Donato, J., Jr., 2021. Rolling out physical exercise and energy homeostasis: Focus on hypothalamic circuitries. Front Neuroendocrinol 63:100944.
[65] Scammell, T.E., Arrigoni, E., Lipton, J.O., 2017. Neural Circuitry of Wakefulness and Sleep. Neuron 93(4):747-765.
[66] Guru, A., Post, R.J., Ho, Y.Y., Warden, M.R., 2015. Making Sense of Optogenetics. Int J Neuropsychopharmacol 18(11):pyv079.

[67] Egan, B., Zierath, J.R., 2013. Exercise metabolism and the molecular regulation of skeletal muscle adaptation. Cell Metab 17(2):162-184.
[68] Sternson, S.M., Atasoy, D., Betley, J.N., Henry, F.E., Xu, S., 2016. An Emerging Technology Framework for the Neurobiology of Appetite. Cell Metab 23(2):234-253.
[69] Zimmerman, C.A., Knight, Z.A., 2020. Layers of signals that regulate appetite. Curr Opin Neurobiol 64:79-88.

Figure 1

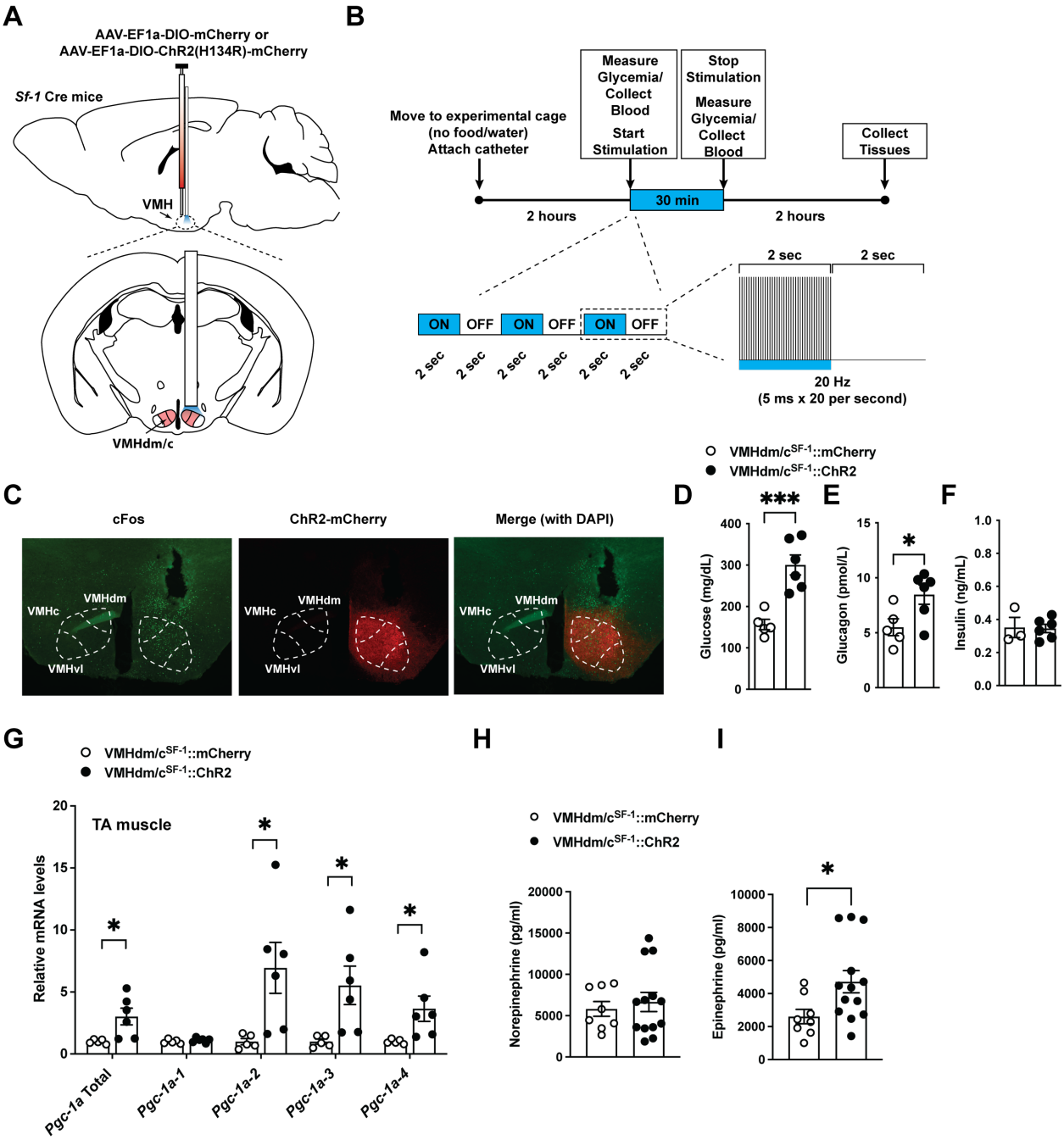
A
AAV-EF1a-DIO-mCherry or
AAV-EF1a-DIO-ChR2(H134R)-mCherry
Sf-1 Cre mice
VMH
VMHdm/c
B
Move to experimental cage
(no food/water)
Attach catheter
Measure
Glycemia/
Collect
Blood
Start
Stimulation
Stop
Stimulation
Measure
Glycemia/
Collect
Blood
Collect
Tissues
2 hours
30 min
2 hours
ON
OFF
ON
OFF
ON
OFF
2 sec
2 sec
2 sec
2 sec
2 sec
2 sec
2 sec
2 sec
20 Hz
(5 ms x 20 per second)
VMHdm/c^SF-1::mCherry
VMHdm/c^SF-1::ChR2
C
cFos
ChR2-mCherry
Merge (with DAPI)
VMHc
VMHdm
VMHvl
D
Glucose (mg/dL)
E
Glucagon (pmol/L)
F
Insulin (ng/mL)
G
TA muscle
Relative mRNA levels
Pgc-1a Total
Pgc-1a-1
Pgc-1a-2
Pgc-1a-3
Pgc-1a-4
H
Norepinephrine (pg/ml)
I
Epinephrine (pg/ml)

Figure 2

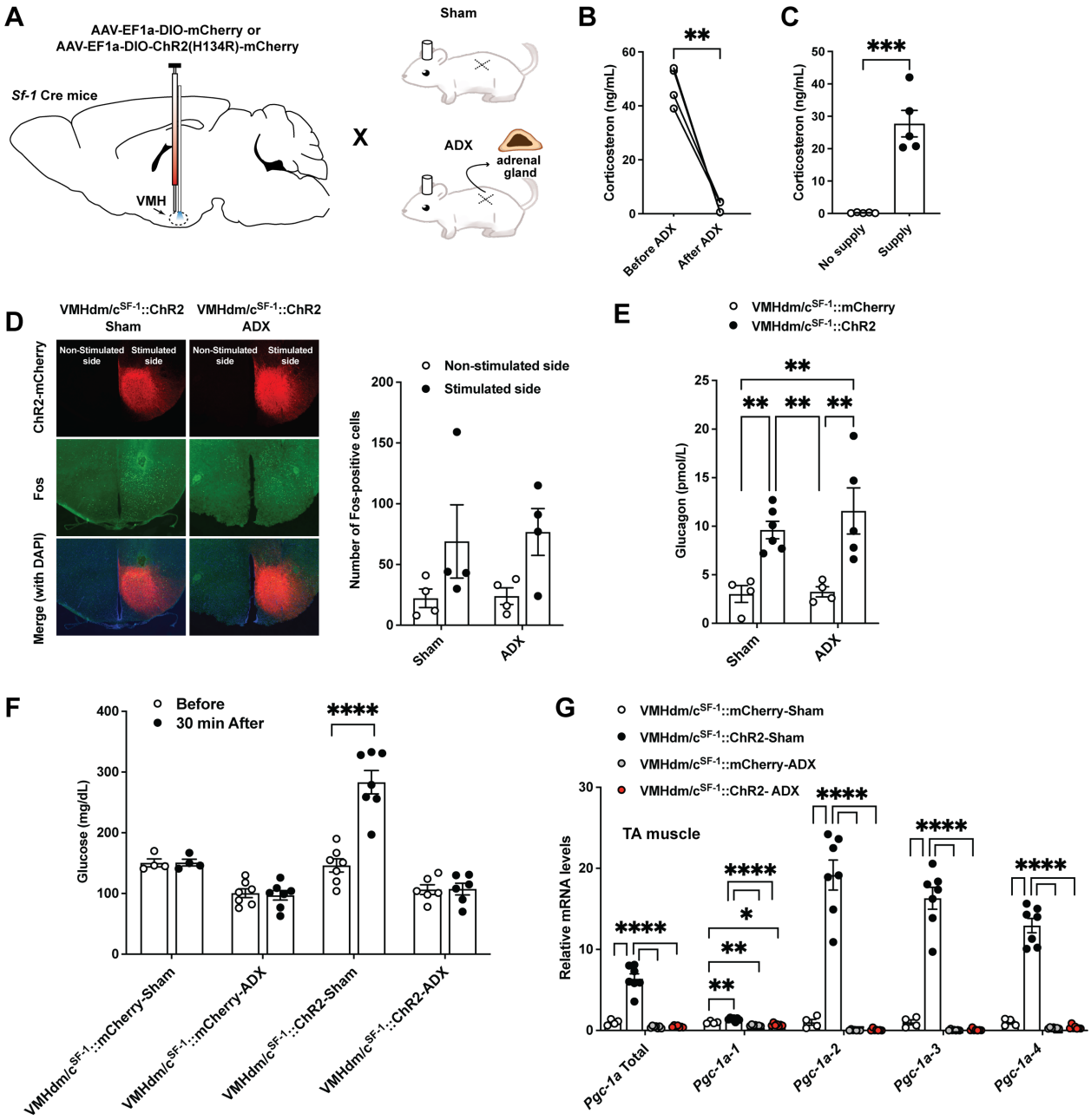
A
AAV-EF1a-DIO-mCherry or
AAV-EF1a-DIO-ChR2(H134R)-mCherry
Sf-1 Cre mice
VMH
X
Sham
ADX
adrenal gland
B
Corticosteron (ng/mL)
Before ADX
After ADX
C
Corticosteron (ng/mL)
No supply
Supply
D
VMHdm/cSF-1::ChR2 Sham
VMHdm/cSF-1::ChR2 ADX
Non-Stimulated side
Stimulated side
ChR2-mCherry
Fos
Merge (with DAPI)
Non-stimulated side
Stimulated side
Number of Fos-positive cells
Sham
ADX
E
VMHdm/cSF-1::mCherry
VMHdm/cSF-1::ChR2
Glucagon (pmol/L)
Sham
ADX
F
Before
30 min After
Glucose (mg/dL)
VMHdm/cSF-1::mCherry-Sham
VMHdm/cSF-1::mCherry-ADX
VMHdm/cSF-1::ChR2-Sham
VMHdm/cSF-1::ChR2-ADX
G
VMHdm/cSF-1::mCherry-Sham
VMHdm/cSF-1::ChR2-Sham
VMHdm/cSF-1::mCherry-ADX
VMHdm/cSF-1::ChR2- ADX
TA muscle
Relative mRNA levels
Pgc-1a Total
Pgc-1a-1
Pgc-1a-2
Pgc-1a-3
Pgc-1a-4

Figure 3

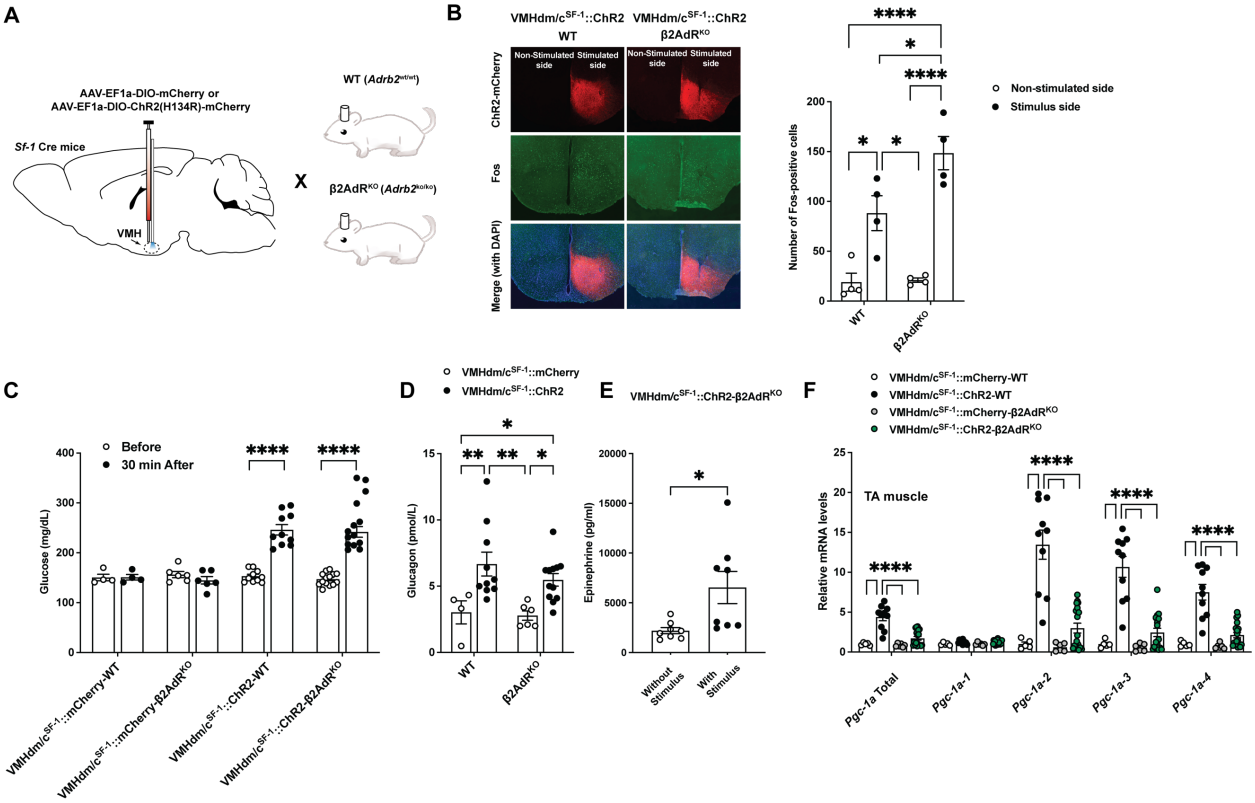
A
AAV-EF1a-DIO-mCherry or
AAV-EF1a-DIO-ChR2(H134R)-mCherry
Sf-1 Cre mice
VMH
X
WT (Adrb2wt/wt)
β2AdRKO (Adrb2ko/ko)
B
VMHdm/cSF-1::ChR2 WT
VMHdm/cSF-1::ChR2 β2AdRKO
Non-Stimulated side
Stimulated side
ChR2-mCherry
Fos
Merge (with DAPI)
Number of Fos-positive cells
Non-stimulated side
Stimulus side
WT
β2AdRKO
C
Before
30 min After
Glucose (mg/dL)
VMHdm/cSF-1::mCherry-WT
VMHdm/cSF-1::mCherry-β2AdRKO
VMHdm/cSF-1::ChR2-WT
VMHdm/cSF-1::ChR2-β2AdRKO
D
VMHdm/cSF-1::mCherry
VMHdm/cSF-1::ChR2
Glucagon (pmol/L)
WT
β2AdRKO
E
VMHdm/cSF-1::ChR2-β2AdRKO
Epinephrine (pg/ml)
Without Stimulus
With Stimulus
F
VMHdm/cSF-1::mCherry-WT
VMHdm/cSF-1::ChR2-WT
VMHdm/cSF-1::mCherry-β2AdRKO
VMHdm/cSF-1::ChR2-β2AdRKO
TA muscle
Relative mRNA levels
Pgc-1a Total
Pgc-1a-1
Pgc-1a-2
Pgc-1a-3
Pgc-1a-4

Figure 4

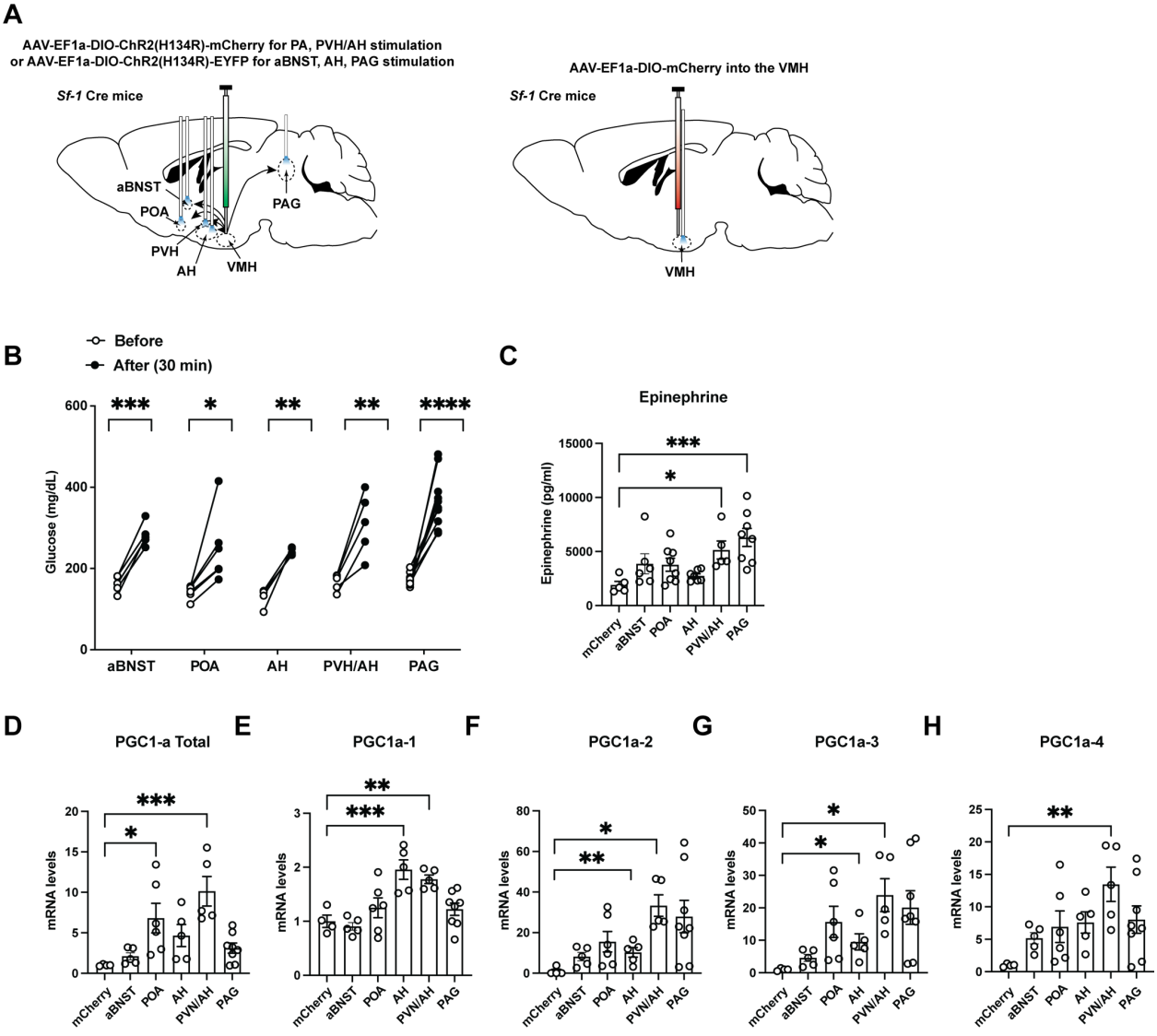
A
AAV-EF1a-DIO-ChR2(H134R)-mCherry for PA, PVH/AH stimulation
or AAV-EF1a-DIO-ChR2(H134R)-EYFP for aBNST, AH, PAG stimulation
Sf-1 Cre mice
aBNST
POA
PVH
AH
VMH
PAG
AAV-EF1a-DIO-mCherry into the VMH
Sf-1 Cre mice
VMH
B
Before
After (30 min)
Glucose (mg/dL)
aBNST
POA
AH
PVH/AH
PAG
C
Epinephrine
Epinephrine (pg/ml)
mCherry
aBNST
POA
AH
PVN/AH
PAG
D
PGC1-a Total
E
PGC1a-1
F
PGC1a-2
G
PGC1a-3
H
PGC1a-4
mRNA levels

Figure 5

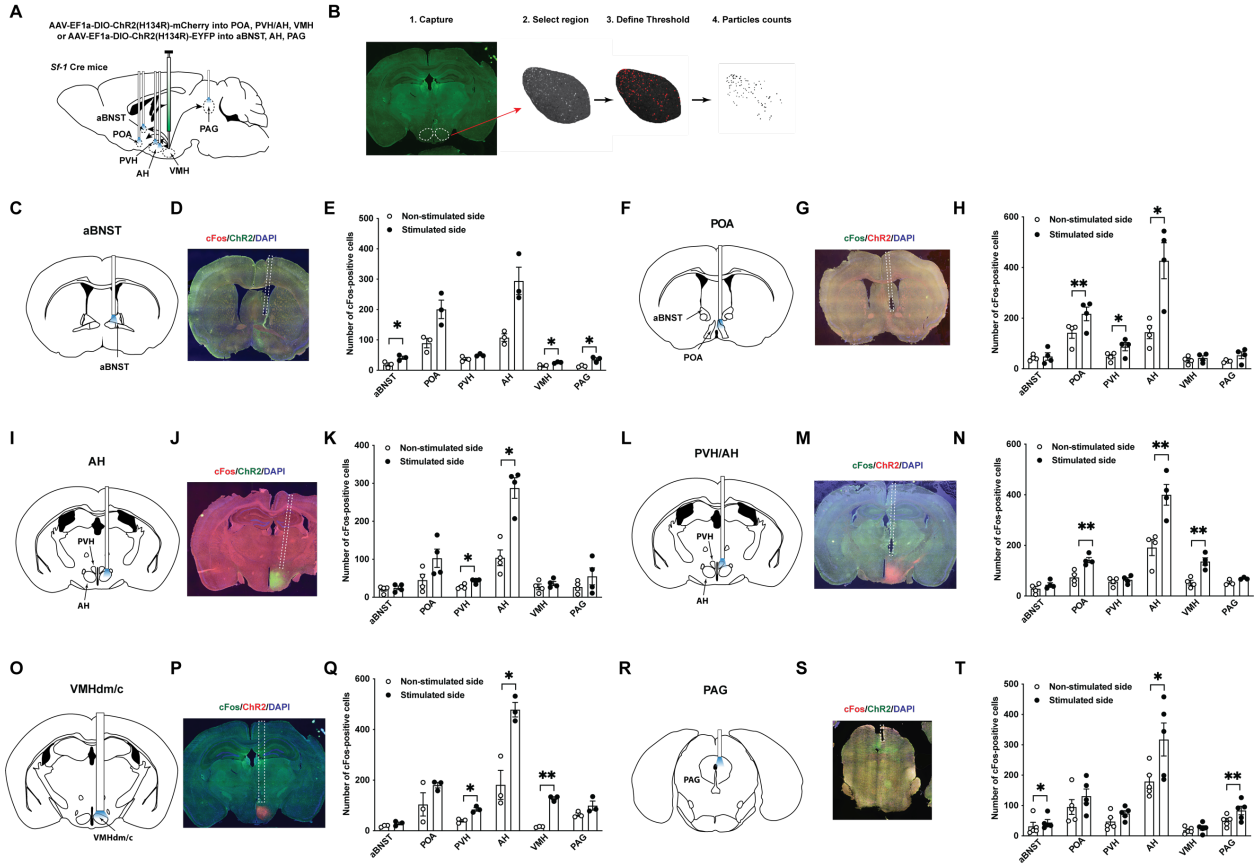
A
AAV-EF1a-DIO-ChR2(H134R)-mCherry into POA, PVH/AH, VMH
or AAV-EF1a-DIO-ChR2(H134R)-EYFP into aBNST, AH, PAG
Sf-1 Cre mice
aBNST
POA
PVH
AH
VMH
PAG
B
1. Capture
2. Select region
3. Define Threshold
4. Particles counts
C
aBNST
D
cFos/ChR2/DAPI
E
Non-stimulated side
Stimulated side
Number of cFos-positive cells
F
POA
G
H
I
AH
J
K
L
PVH/AH
M
N
O
VMHdm/c
P
Q
R
PAG
S
T

S Figure 1

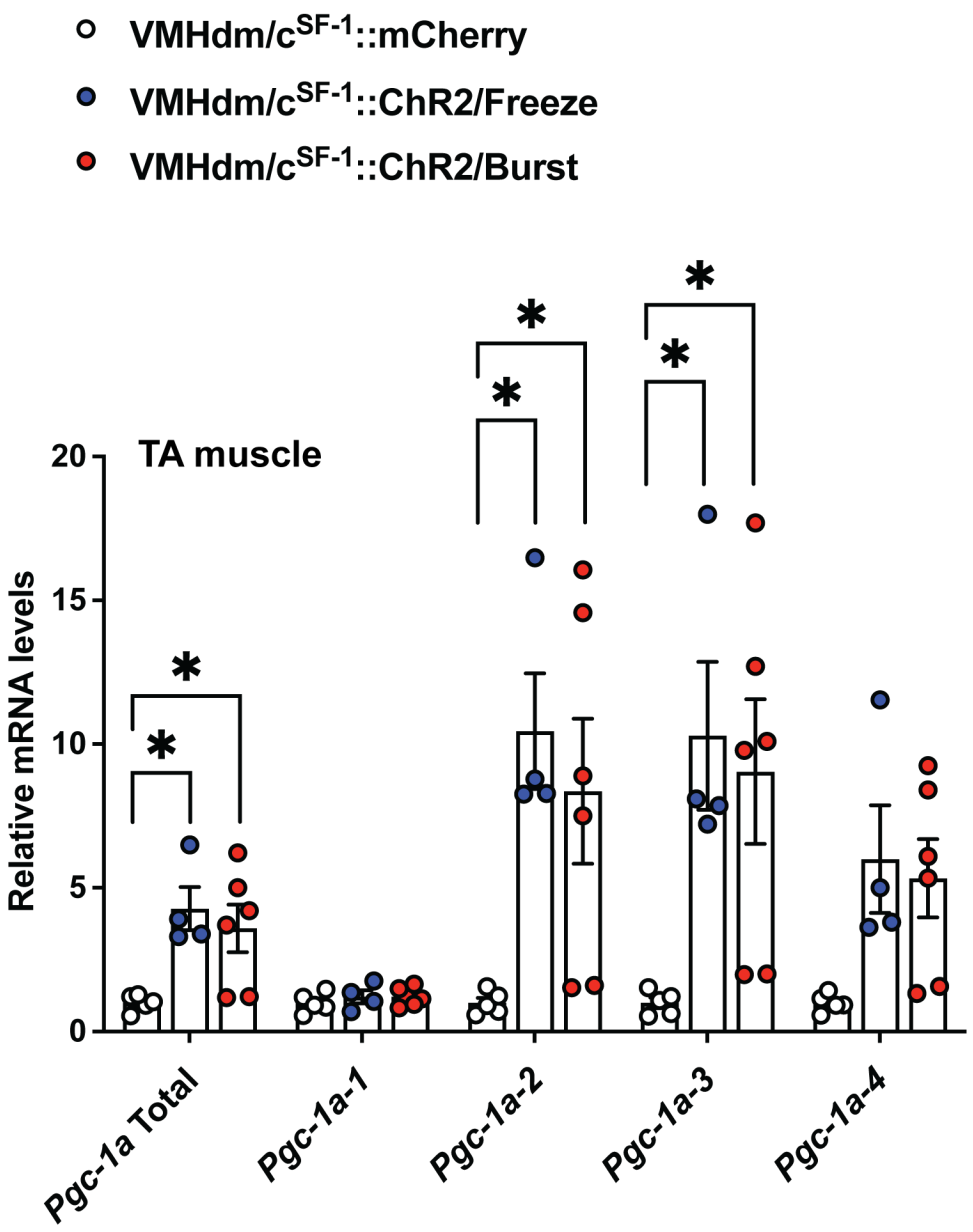
VMHdm/c^{SF-1}::mCherry
VMHdm/c^{SF-1}::ChR2/Freeze
VMHdm/c^{SF-1}::ChR2/Burst
TA muscle
Relative mRNA levels
20
15
10
5
0
*
Pgc-1a Total
Pgc-1a-1
Pgc-1a-2
Pgc-1a-3
Pgc-1a-4

S Figure 2

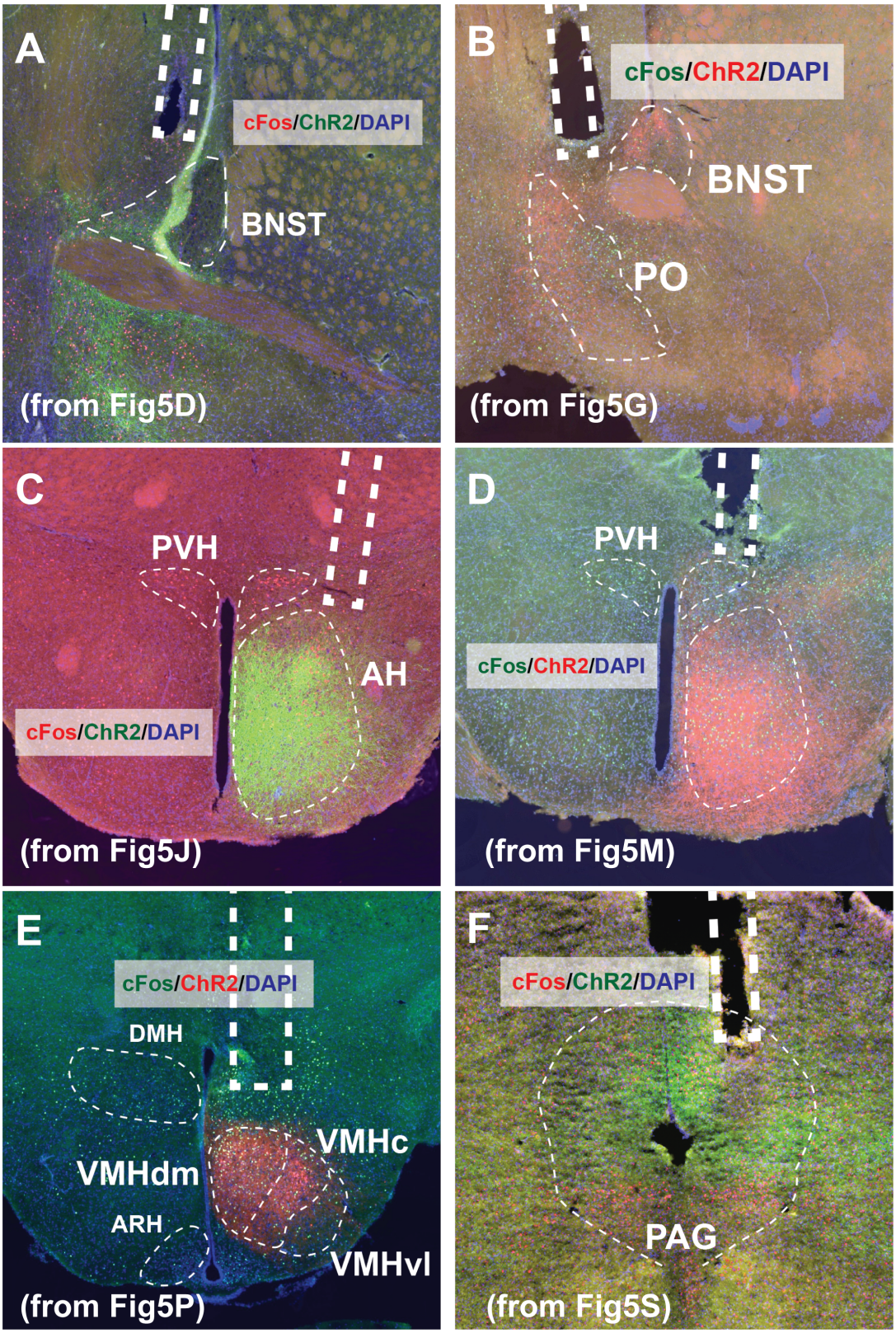
A
cFos/ChR2/DAPI
BNST
(from Fig5D)
B
cFos/ChR2/DAPI
BNST
PO
(from Fig5G)
C
PVH
AH
cFos/ChR2/DAPI
(from Fig5J)
D
PVH
cFos/ChR2/DAPI
(from Fig5M)
E
cFos/ChR2/DAPI
DMH
VMHc
VMHdm
ARH
VMHvl
(from Fig5P)
F
cFos/ChR2/DAPI
PAG
(from Fig5S)

S Figure 3

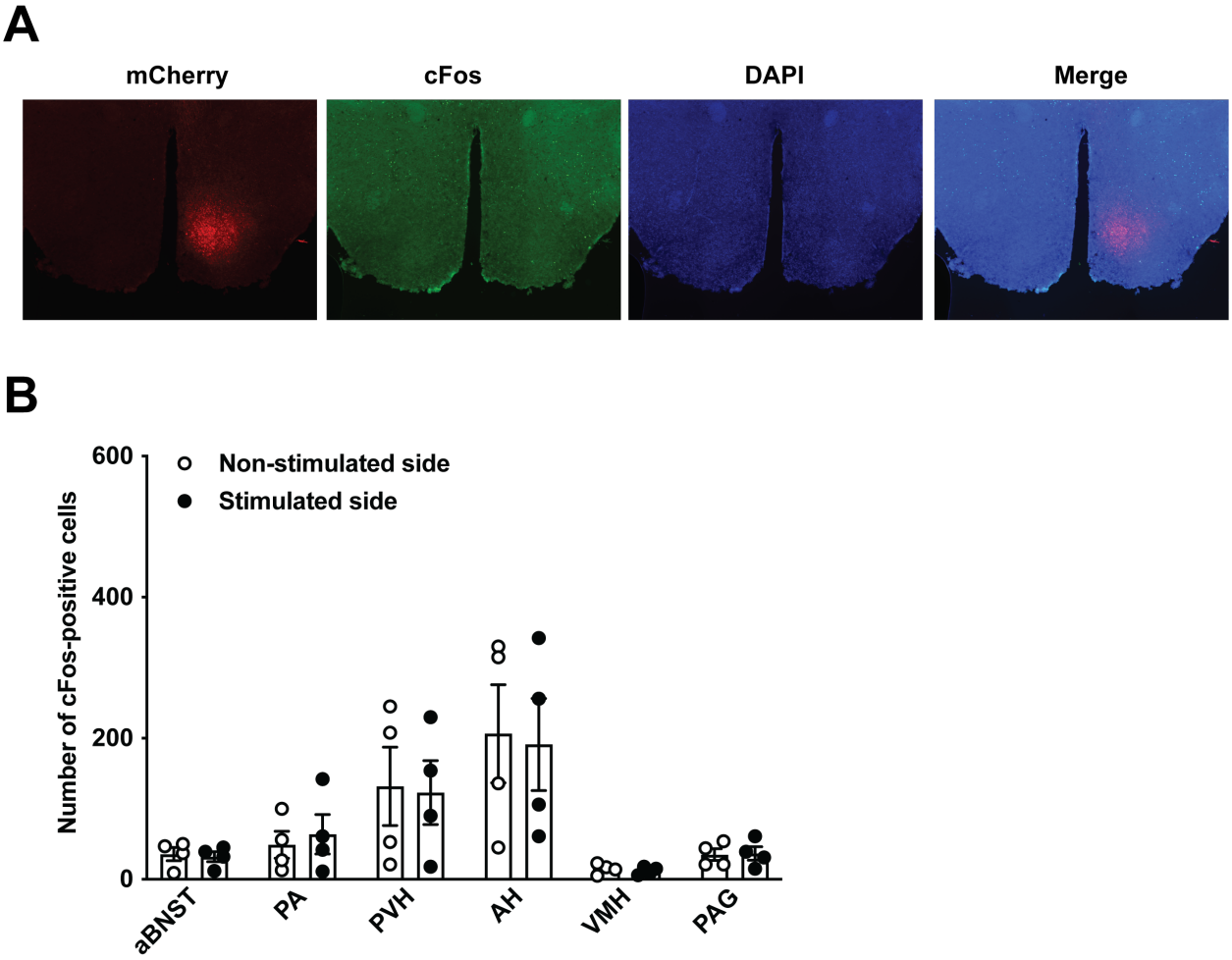
A
mCherry
cFos
DAPI
Merge
B
Non-stimulated side
Stimulated side
Number of cFos-positive cells
600
400
200
0
aBNST
PA
PVH
AH
VMH
PAG

S Figure 4

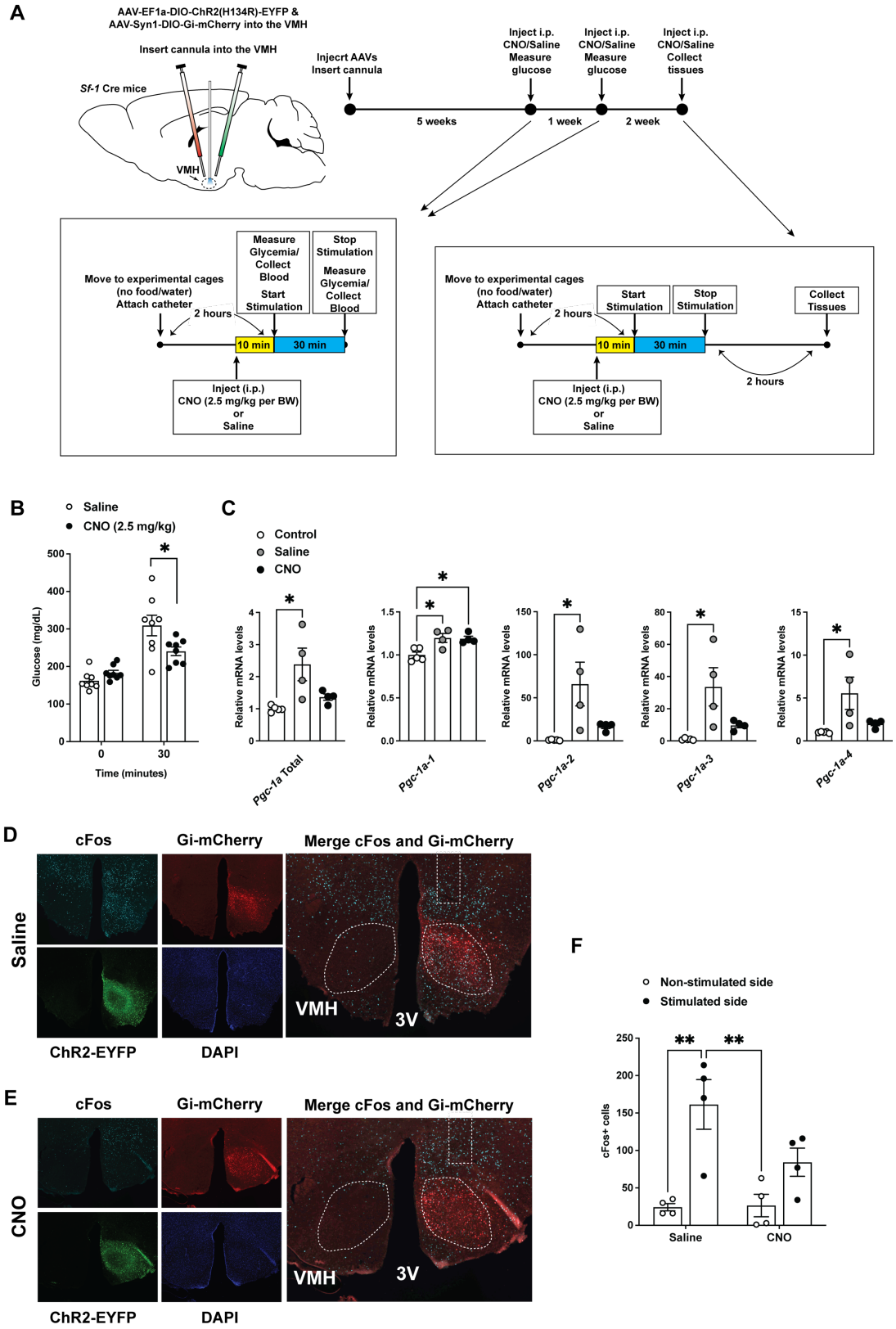
A
AAV-EF1a-DIO-ChR2(H134R)-EYFP &
AAV-Syn1-DIO-Gi-mCherry into the VMH
Insert cannula into the VMH
Sf-1 Cre mice
VMH
Injecrt AAVs
Insert cannula
Inject i.p.
CNO/Saline
Measure
glucose
Inject i.p.
CNO/Saline
Measure
glucose
Inject i.p.
CNO/Saline
Collect
tissues
5 weeks
1 week
2 week
Move to experimental cages
(no food/water)
Attach catheter
2 hours
Measure
Glycemia/
Collect
Blood
Start
Stimulation
Stop
Stimulation
Measure
Glycemia/
Collect
Blood
10 min
30 min
Inject (i.p.)
CNO (2.5 mg/kg per BW)
or
Saline
Move to experimental cages
(no food/water)
Attach catheter
2 hours
Start
Stimulation
Stop
Stimulation
Collect
Tissues
10 min
30 min
2 hours
Inject (i.p.)
CNO (2.5 mg/kg per BW)
or
Saline
B
Saline
CNO (2.5 mg/kg)
Glucose (mg/dL)
Time (minutes)
C
Control
Saline
CNO
Relative mRNA levels
Pgc-1a Total
Pgc-1a-1
Pgc-1a-2
Pgc-1a-3
Pgc-1a-4
D
cFos
Gi-mCherry
Merge cFos and Gi-mCherry
Saline
VMH
3V
ChR2-EYFP
DAPI
E
cFos
Gi-mCherry
Merge cFos and Gi-mCherry
CNO
VMH
3V
ChR2-EYFP
DAPI
F
Non-stimulated side
Stimulated side
cFos+ cells
Saline
CNO

S Figure 5

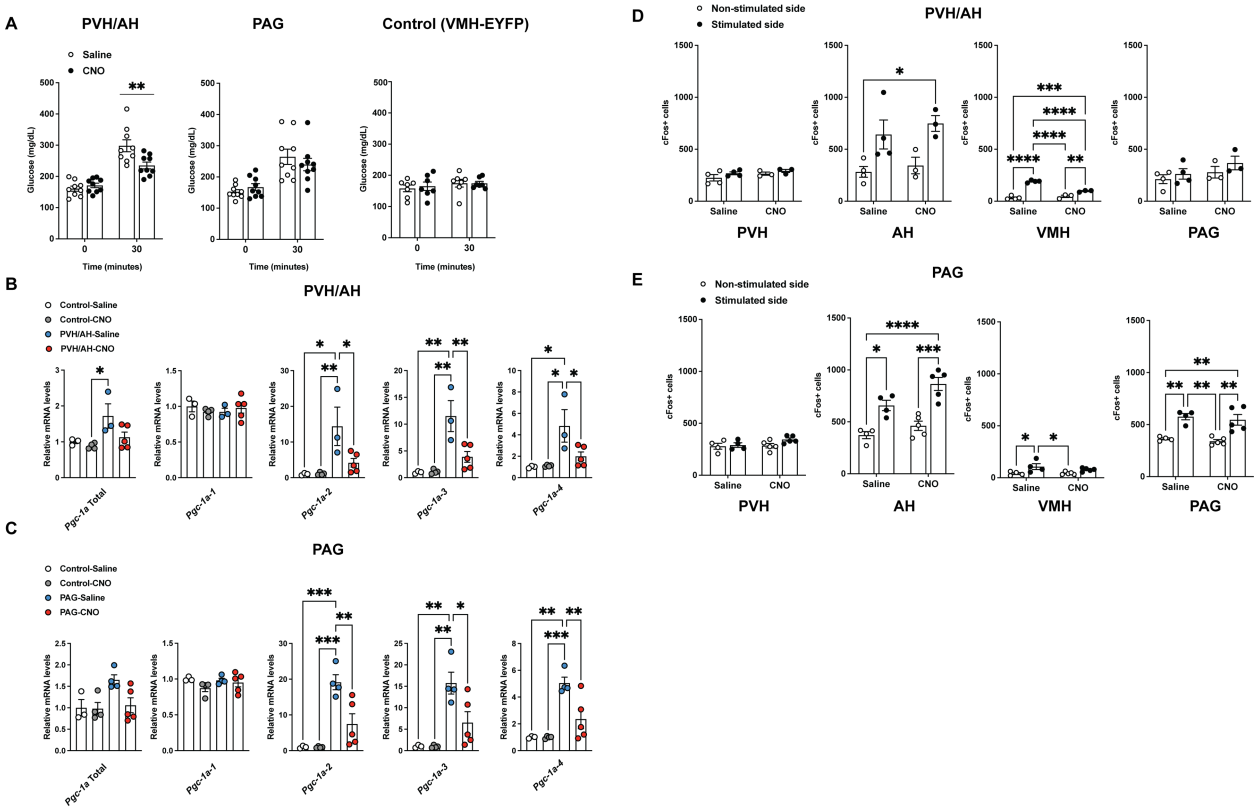
A
PVH/AH
PAG
Control (VMH-EYFP)
Saline
CNO
Glucose (mg/dL)
Time (minutes)
B
PVH/AH
Control-Saline
Control-CNO
PVH/AH-Saline
PVH/AH-CNO
Relative mRNA levels
Pgc-1a Total
Pgc-1a-1
Pgc-1a-2
Pgc-1a-3
Pgc-1a-4
C
PAG
Control-Saline
Control-CNO
PAG-Saline
PAG-CNO
D
PVH/AH
Non-stimulated side
Stimulated side
cFos+ cells
Saline
CNO
PVH
AH
VMH
PAG
E
PAG

S Figure 6

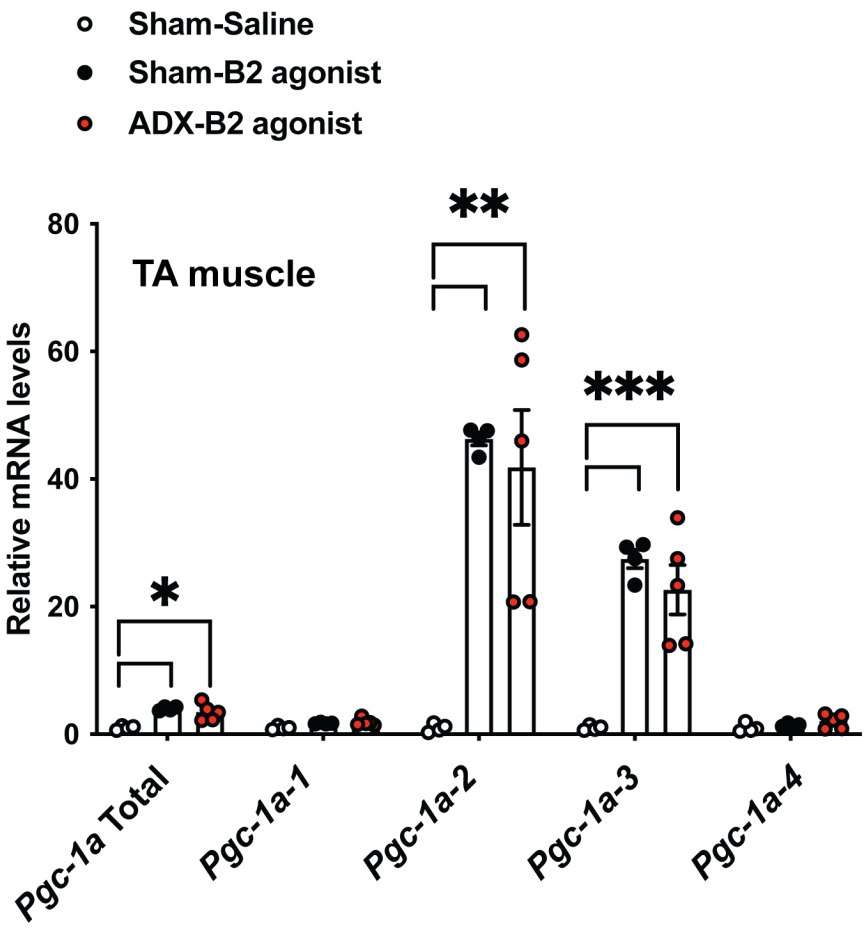
Sham-Saline
Sham-B2 agonist
ADX-B2 agonist
TA muscle
Relative mRNA levels
80
60
40
20
0
*
**
***
Pgc-1a Total
Pgc-1a-1
Pgc-1a-2
Pgc-1a-3
Pgc-1a-4

S Figure 7

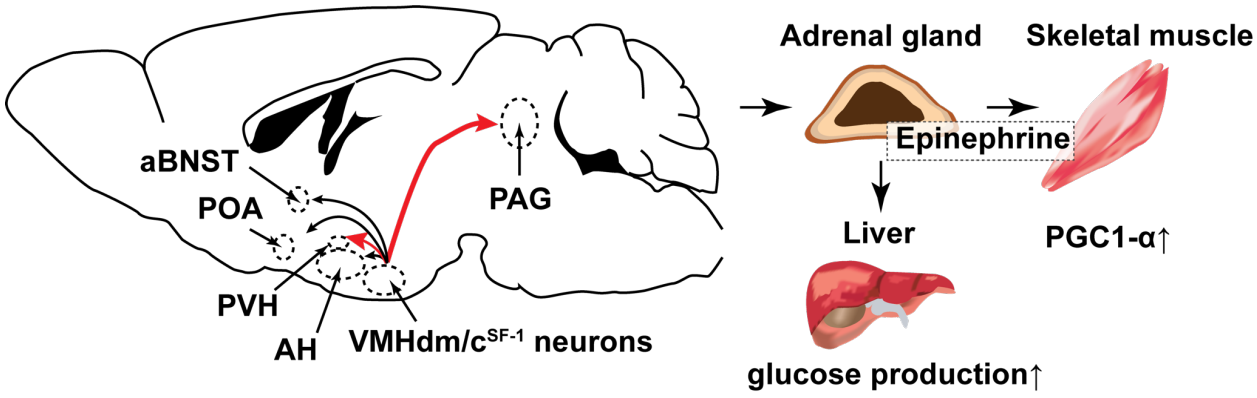
aBNST
POA
PVH
AH
VMHdm/c^{SF-1} neurons
PAG
Adrenal gland
Skeletal muscle
Epinephrine
Liver
PGC1-α↑
glucose production↑